Two-brain microstates: A novel hyperscanning-EEG method for quantifying task-driven inter-brain asymmetry

Qianliang Li[1*], Marius Zimmermann[1,2] and Ivana Konvalinka[1]

[1]Section for Cognitive Systems, DTU Compute, Technical University of Denmark, Kongens Lyngby, Denmark,

[2]Institute of Psychology, University of Regensburg, Regensburg, Germany,

[*]Corresponding author. Email: glia@dtu.dk

ABSTRACT

Joint action and interpersonal coordination between individuals are integral parts of daily life, and various behavioral tasks have been designed to study their emergence and maintenance. One example is the mirror-game paradigm, which examines the dynamics of two people improvising motion together. However, the underlying neural mechanisms remain poorly understood, and inter-brain methods underdeveloped. Previously, we reported unique individual behavioral and neural signatures of performing actions when observed by others using a mirror-game paradigm. Here, we explored inter-brain synchronization during the mirror-game paradigm using a novel approach employing two-brain EEG microstates. Microstates are quasi-stable configurations of brain activity that have been reliably replicated across studies, and proposed to be basic buildings blocks for mental processing. Expanding the microstate methodology to dyads of interacting participants (two-brain microstates) enables us to investigate quasi-stable moments of inter-brain synchronous and asymmetric activity. Interestingly, we found that conventional microstates fitted to individuals were not related to the different task conditions; however, the dynamics of the two-brain microstates were changed for the observed actor-observer condition, compared to all other conditions where participants had more symmetric task demands (rest, individual, joint). These results suggest that two-brain microstates might serve as a method for identifying inter-brain states during asymmetric real-time social interaction.

***Keywords*:** EEG, Hyperscanning, Microstate, Mirror-game, Source localization

1 Introduction

To fully understand social cognition between individuals interacting together, it has been argued that it is inadequate to only measure neural processes in single, isolated individuals. Instead, a second-person approach should be employed to capture both the neural processes within individuals engaged in interaction, but also the dynamic interactions and processes between individuals (Schilbach et al., 2013; Konvalinka and Roepstorff, 2012; Dumas, 2011; De Jaegher et al., 2010; Dingemanse et al., 2023). The interpersonal and inter-brain mechanisms tap into important aspects of social processes that evolve over time between interacting partners, as well as more fine-grained mechanisms of coordination (Konvalinka and Roepstorff, 2012; Konvalinka et al., 2023). In the last two decades, the simultaneous measurement of brain activity from multiple individuals (using multi-person EEG, MEG, fNIRS or fMRI recordings) has become one particular trend that has emerged in quantifying the interpersonal, dynamic neural mechanisms between interacting individuals, and has been coined hyperscanning (Montague et al., 2002). A growing body of hyperscanning studies has shown that people's brain rhythms or activities synchronize when they engage in social interaction with each other (see Babiloni and Astolfi (2014); Czeszumski et al. (2020) for reviews), while e.g., coordinating or synchronizing their actions (Dumas et al., 2010; Zamm et al., 2018; Lindenberger et al., 2009), cooperating with one another (Hu et al., 2018; Cui et al., 2012), turn-taking in verbal interaction (Ahn et al., 2018), or while merely able to see each other in unstructured tasks (Koul et al., 2023). However, while hyperscanning has been around for two decades,

with growing efforts to standardise the methodology (Ayrolles et al., 2021), the inter-brain analysis methods remain underdeveloped, lacking clear standards (Zamm et al., 2024; Zimmermann et al., 2024), and primarily focused on measuring synchrony between people's neural signals, drawing critique with respect to the underlying functional significance of inter-brain synchrony (IBS) (Hamilton, 2021; Holroyd, 2022). Hence, more innovative inter-brain methods are required to go beyond IBS, to potentially also examine the interpersonal asymmetry in neural mechanisms - i.e., processes that enable or underlie different social tasks, roles, and interaction strategies, which emerge between people when they interact with each other. Asymmetric interaction behaviour may include e.g., taking on leader or follower roles when coordinating actions, producing complementary rather than imitative actions, initiating versus mimicking behaviour, or observing versus being observed (Sebanz et al., 2006; Konvalinka et al., 2023). While inter-brain synchrony may still underlie such asymmetric behaviour, there may be important functionally relevant differences in neural processes between participants with different roles in e.g., action-perception coupling, which are poorly understood.

For example, previous work has shown that asymmetric leader-follower roles emerge when people interact with one another, and that they can be predicted based on 10 Hz oscillations measured using dual-EEG, when employing two-brain analyses (Konvalinka et al., 2014). In this study, participants engaged in an interactive finger-tapping task with each other or with a computer metronome. When applying multivariate decoding techniques to the two-brain data, the 10 Hz power across only the leaders' frontal electrodes were picked up as reliable classifiers of interactive versus non-interactive conditions. As leaders had to suppress the sounds they heard from the other person and focus more on monitoring their own taps, this suggests that suppression of frontal 10 Hz power may be a potential neural mechanism underlying leading, or increased self-monitoring, behaviour. Meanwhile, followers exhibited more similar frequency power modulations between interactive and non-interactive conditions, given that they were following the other person or the computer, respectively. Notably, this neural asymmetry was only picked up when using dual-EEG data, rather than focusing on individual neural modulations.

Another study investigating role-differences between senders and receivers in a cooperative game found an asymmetry in alpha and low beta event-related desynchronization between the senders and receivers (Flösch et al., 2023). Here, the participants engaged in a cooperative Pacman Game, where one participant (the sender) sent information about the correct moving direction in the form of a picture cue to the other player (the receiver), who had to correctly decode the picture cue in order to move towards the goal. The receiver exhibited a larger alpha/beta power decrease compared to the sender, potentially indicating higher cognitive demands, in line with the role asymmetry which required the receiver to represent more information than the sender.

Other studies have also identified asymmetric inter-brain functional connectivity patterns between players during a 4-person card game (Babiloni et al., 2007; Astolfi et al., 2010). Here, the two versus two player game required both cooperation within two-person teams, and competition between teams. By using partial directed coherence, which is a Granger-causality approach in the frequency domain that describes the connectivity between two time-series after discounting the influences from all other $N - 2$ time series (Baccalá and Sameshima, 2001), the authors found asymmetric directed (i.e., Granger-causal) coherence between the prefrontal Brodmann areas 8 and 9/46 of one player, and the anterior cingulate cortex (ACC) of their partner (Astolfi et al., 2010). Notably, this coherence was only found between the members of the same team.

In addition to having different roles in social interaction, such as that of a leader and follower, or sender and receiver, people may also adopt different interpersonal strategies. For example, people may choose to adapt to each other as mutual followers, or mutually decide to ignore one another, exhibiting so-called leader-leader behaviour (Heggli et al., 2021). Such different interpersonal strategies during real-time social coordination have been shown to emerge between musicians, and have different underlying neural networks. E.g., mutual adaptation exhibits more frequent occurrence of phase-locked activity in the alpha frequency band within the right temporoparietal network compared to leader-leader behaviour, presumably showing more recruitment of action-perception neural networks. However, these differences were found using single-brain analyses; hence, it is unclear whether there

were additional inter-brain asymmetries.

In this paper, we were interested in exploring both synchronized as well as unexplored asymmetric neural mechanisms during social interaction, by developing a novel two-brain microstates method, which could be freely applied to interaction conditions that involve both symmetric and asymmetric tasks and roles. Microstates are quasi-stable configurations of brain activity that have been reliably replicated across studies, and proposed to be basic buildings blocks for mental processing (Lehmann et al., 1987; Michel and Koenig, 2018). A growing number of studies have employed microstates to investigate the neural correlates of cognitive processes and clinical disorders, e.g. schizophrenia, psychosis, Alzheimer's disease, epilepsy, bipolar disorder, autism spectrum disorder and many others (reviewed in Michel and Koenig (2018); Tarailis et al. (2023)). Expanding the microstate methodology to dyads of interacting participants (two-brain microstates) enables us to investigate quasi-stable moments of inter-brain synchronized activity, while not constraining the quantification of inter-brain synchronization to symmetric brain states. In other words, a single two-brain microstate could be asymmetric for the two participants in a dyad, if that particular combination of asymmetric brain states often occurred simultaneously in the dyads. This feature enables two-brain microstates to potentially uncover contrasting patterns of brain activity when people engage in symmetric versus asymmetric interactive tasks.

To evaluate the functional role of two-brain microstates, we applied this new method to hyperscanning EEG data from an experiment employing the adapted mirror game paradigm (Zimmermann et al., 2022). The mirror game paradigm engages pairs of participants in an improvised movement game, where they are asked to improvise motion together by creating synchronized and interesting movements (Noy et al., 2011). The participants had to perform horizontal finger movements by moving a slider, and we manipulated whether the participants could see each other's hand. The participants thus produced horizontal movements across a number of conditions involving symmetric, but not necessarily interactive tasks: independent movements (uncoupled condition), interactive movements (coupled condition), similar but not interactive movements while both synchronized to the same pre-recorded signal (control condition). They also engaged in two asymmetric interactive conditions where they either had asymmetric roles or asymmetric tasks: where one was assigned the role of a leader and the other of a follower (follower-leader condition), and where one was told to improvise independent movements while observed by the other (observer-actor condition). Figure 1 shows a schematic of the experiment.

Previously, we conducted intra-brain analyses on this data set, and reported unique individual behavioral and neural signatures when performing actions when observed by others (Zimmermann et al., 2022). Zimmermann et al. (2022) showed that participants produced movements that were slower, less variable, but more exaggerated in amplitude, when they were observed by the other person, compared to when they were unable to see each other, indicating audience effects. In addition, observed actions were characterized by increased widespread functional connectivity in the alpha frequency range in contrast to both individual (uncoupled) and interactive (coupled) actions, potentially indicating increased self-monitoring and focus.

In order to explore inter-brain mechanisms across the different symmetric and asymmetric interaction conditions, we applied our novel two-brain EEG microstates method. We hypothesized that the coupled condition would lead to higher inter-brain synchronization than the other conditions (particularly the non-interactive ones), based on previous research; and that asymmetric conditions (follower-leader, observer-actor) would lead to more pronounced asymmetries between the two persons' brains compared to the coupled condition, which would be captured with two-brain microstate dynamics. Crucially, we also investigated whether microstate dynamics would be better differentiated across the different interaction conditions when they were fitted to two-brains rather than individual brains.

2 Materials and Methods

2.1 Dataset

The data have been previously described in Zimmermann et al. (2022). Originally, 25 pairs were recruited to participate in a mirror-game paradigm while simultaneous EEG was recorded. The pairs consisted of 11 mixed-sex, and 14 same-sex pairs (1 female-female, 13 male-male). 16 pairs were friends/partners, and 9 pairs did not know each other before

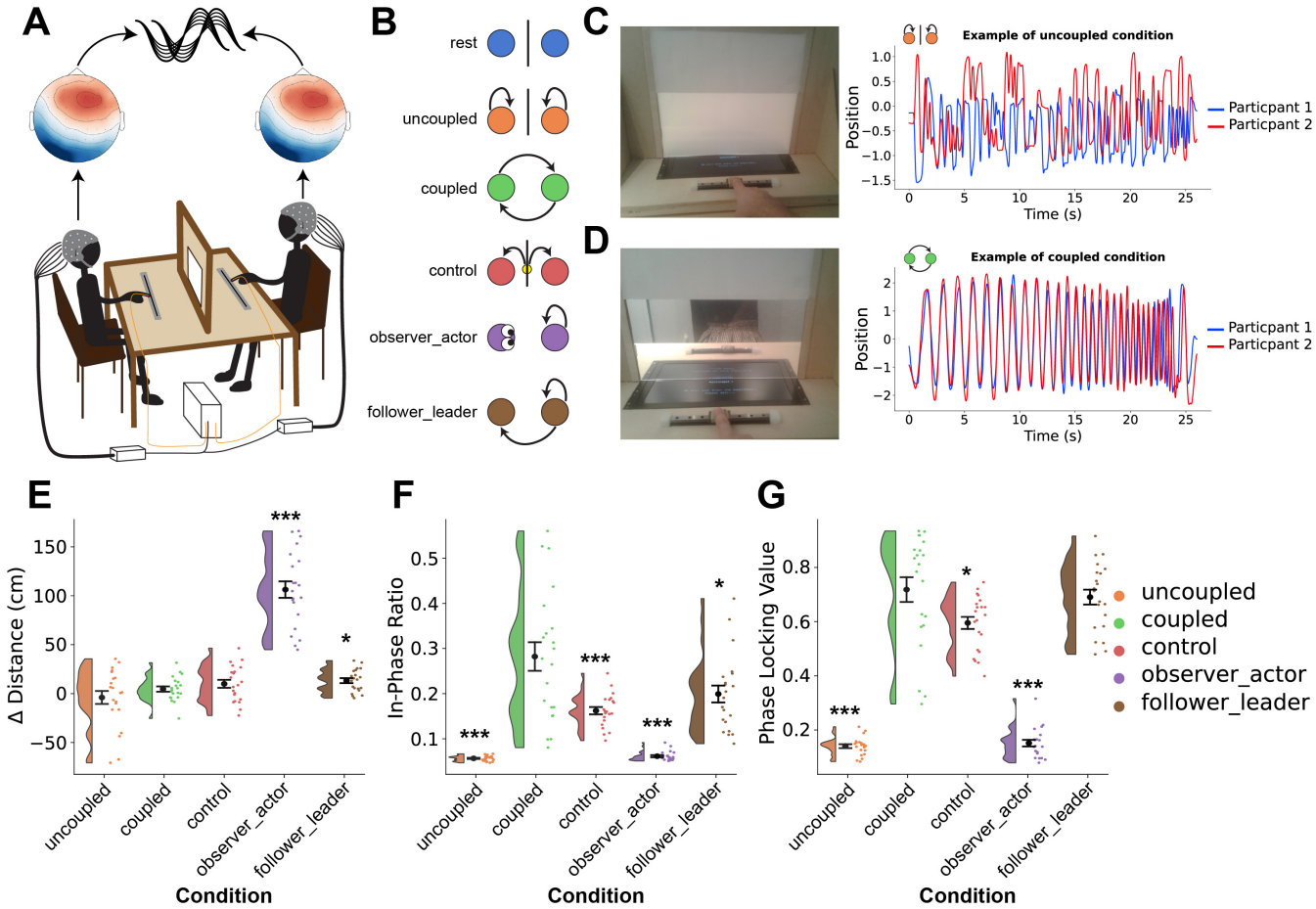

Fig. 1. **Overview of the mirror-game setup and the different behavioral conditions.** A) Dyads performed the mirror-game paradigm, during which we measured their EEG. The two-brain EEG data were subsequently analyzed using microstate analysis and inter-brain synchronization was estimated. B) The dyads performed four types of symmetric (rest, uncoupled, coupled and control) and two asymmetric (observer-actor and follower-leader) conditions. C) Example of the non-interactive uncoupled condition and the finger positions of each participant. D) Example of the interactive coupled condition, with strong behavioral synchronization. E-G) Behavioral performance measures for each condition. All statistical tests were performed in contrast to the principal interactive coupled condition. E) The asymmetric conditions had a greater difference in distance moved compared to the coupled condition, indicating the actor and leader moved more than the observer and follower, respectively. The coupled condition displayed the highest behavioral synchrony, as measured by F) the ratio of time the finger movements were in-phase (within 10° from each other) and G) the phase locking value, followed by the follower-leader and control conditions, with uncoupled and observer-actor conditions displaying minimal synchrony. Adapted from Zimmermann et al. (2022).

the experiment, but were introduced to each other during preparations of the experiment. Due to technical problems during the experiment and EEG data quality issues, four pairs were dropped, hence 21 pairs (42 participants; 26% female; aged 20-33, 24.36 years on average) were included in the analysis.

The mirror-game is an experimental paradigm designed for examining the dynamics of two interacting individuals (Noy et al., 2011), where the two participants improvise motion either alone or together with a partner. The participants were divided by a liquid crystal screen, which could be turned off during non-interactive conditions (Figure 1C) or on during interactive conditions (Figure 1D), manipulating whether participants had visual feedback of each other's movements or not. The vision of their partner's face and body was always blocked. The participants thus produced horizontal movements across a number of conditions involving symmetric, but not necessarily interactive tasks: 1) 2 min *rest* condition

at the start and end of experiment (screen off), 2) 16×25 sec *uncoupled* movements where participants could not see each other and produced independent movements (screen off), 3) 16×25 sec *coupled* movements where participants could see each other and synchronized their movements (screen on), 4) 16×25 sec *control* condition where participants had to follow a dot on the screen (screen off), hence interacting with the same stimulus but not with each other (the movement of the dot corresponded to movements produced in the coupled condition of pilot participants), 5) $2 \times 8 \times 25$ sec *observer-actor* with one participant producing improvised movements while observed by the (non-moving) partner (screen on), and 6) $2 \times 8 \times 25$ sec *follower-leader* where each participant was designated a specific role, while able to see each other (screen on). Specifically, participants were instructed to produce free movements either alone (*uncoupled*) or synchronized without a designated leader (*coupled*). In the *follower-leader* condition, the leader was instructed to produce free movements, while the follower was instructed to imitate (mirror) these movements. For the *observer-actor* condition, the actor was instructed to produce free movements, while the observer was instructed to observe. Finally, in the *control* condition both participants were asked to imitate (mirror) the dot movements on the screen, which was the same (but mirrored) for both participants - hence a control for the similarity in movements produced in the coupled condition, without the interpersonal interaction. Each trial was preceded by a short label informing about the upcoming condition, and, where applicable, the role of each participant. Trial order was pseudo-randomized, such that each block of five trials contained all experimental conditions, and conditions did not repeat in consecutive trials. For the observer-actor and follower-leader conditions, the assigned roles were alternated between participants. Figure 1 shows a schematic of the experiment.

2.2 Movement data analysis

The finger movements were recorded using Polhemus LIBERTY and pre-processed as described in Zimmermann et al. (2022). To estimate the behavioral performance of each dyad, i.e. their movement synchronization, the following behavioral features were computed from their finger positions over time: the difference in distance moved between the interacting participants, the amount of time their movements were in-phase (defined as being within $10°$), and the phase locking value (Lachaux et al., 1999). The Hilbert transform was utilized to estimate the phase of each person's movement time series.

2.3 EEG preprocessing

The EEG was recorded and pre-processed as described in Zimmermann et al. (2022). Briefly, two synchronized 64-channel Biosemi EEG set-ups were recorded at a 2 kHz sampling frequency, followed by bandpass filtering at 1-40 Hz, and downsampling to 256 Hz. Manual visual inspection was performed to clean the data, and independent component analysis (ICA) was used to correct for eye movements and eye blinks.

2.4 Microstate analysis

Microstates are typically estimated in broadband, but a recent paper (Férat et al., 2022) demonstrated the value of spectrally specific microstates and given previous literature showing that alpha and beta oscillations are modulated during motor interactions (Klimesch et al., 2007; Tognoli et al., 2007; Dumas et al., 2012; Conway et al., 1995; Perez et al., 2006; Baker, 2007), we estimated the microstates in the alpha (8-13 Hz), beta (13-30 Hz) and broadband (1-40 Hz) frequency ranges. Single-brain microstate analysis was performed using the open-source EEG microstate python package by von Wegner and Laufs (2018). Briefly, EEG from all individuals were concatenated along the time axis, in order to fit the microstates over all the subjects and obtain the same topographic maps. Global field power (GFP) was computed and EEG topographies at local GFP maxima were clustered using the modified K-means algorithm (Pascual-Marqui et al., 1995). We ran K-means 100 times with 3 to 10 clusters and used the cross-validation criterion (Pascual-Marqui et al., 1995) to determine the final number of clusters. The determined microstate topographies were competitively fitted back into the EEG data sets to yield time series of microstate sequences. The following commonly used microstate features were estimated: ratio of time covered (relative time a microstate is active as a ratio of the total time), duration (mean duration a given microstate remains stable, i.e. occur consecutively), occurrence (mean number of times a microstate occurred during a one second period), transition matrices (mean probability of transitioning from one microstate to itself or another) and entropy (Shannon entropy) were computed for the microstates (von Wegner and Laufs, 2018; Tarailis et al., 2023).

One definition of inter-brain synchronization is that the two brains are displaying similar activity at the same times. To investigate whether the participants of the mirror-game exhibited this form of synchronized activity, we quantified how often the dyads were in the exact same single-brain microstates at the same times, and looked at the dynamics of this co-occurrence of quasi stable global brain activity for the different behavioral conditions. Specifically, we created an inter-brain microstate sequence time series based on the intersection at each time point of the two individual microstate sequence time series from a dyad. In other words, if both brains are in microstate A at the same time point, then the inter-brain microstate sequence time series at that time point will also be A, however if their labels are different, then they do not intersect and we labeled it arbitrarily as Z to denote zero inter-brain synchrony.

However, the criteria of being in the exact same global neural activity state might be too strict, so we also worked with two less constrained definitions of inter-brain synchronization. In the first implementation, we allowed for time-lags to shift either participant 1 or 2's microstate sequence time series with up to 1 second in both directions, in order to determine a specific lag that had the highest amount of time-shifted inter-brain synchronization (comparable to cross-correlation). In the second implementation we removed the constraint of the two brains in a dyad being in the exact same state, and as long as the two potentially different states consistently co-occurred over time, we considered them to be synchronized. This definition of inter-brain synchronization gave rise to what we refer to as two-brain microstates, where each two-brain microstate consists of a fixed global neural activity pattern, which can be different for the two individuals. To implement it in practice, we concatenated the EEG data from each pair along the channel axis, before concatenating all the dyads along the time axis. By concatenating over the channel axis as opposed to the time axis for the two participants in a dyad, we allowed the two-brain microstates to have different topographies for each person in a dyad as long as they occurred simultaneously, i.e., a two-brain microstate could be asymmetric. Note that a two-brain microstate thus consist of activity in 128 channels, but for visualization we plotted the electrodes corresponding to each individual separately to show their topographies, but it is in fact one "inter-brain state". Additionally, there was no issue of electrode adjacency when concatenating over the channel axis, as the K-means algorithm do not take into account the order of the dimensions (channels) of the data. To retain the polarity invariance in two-brain microstates, we computed the spatial correlation for all four combinations of possible polarity configurations for the two brains and used the highest correlation (see discussion for more details). We also estimated long-range temporal correlations using detrended fluctuation analysis (DFA) to compute the Hurst exponent (Hardstone et al., 2012).

2.5 Source localization

We utilized eLORETA, as implemented by MNE-Python v1.3.1 (Gramfort et al., 2013), to obtain cortical current estimates for the two-brain microstates. The FreeSurfer average brain template from FreeSurfer 6 (Fischl, 2012) was used to construct the boundary element head model and forward operator for the source modelling. The regularization parameter was set to $\lambda^2 = 1/9$ and we used the normal orientation, i.e. only the portion of the activity perpendicular to the cortex. The time series of the 20484 source vertices were further collapsed into 68 cortical patches based on the Desikan Killiany atlas, by first aligning the dipole orientations by shifting vertices with opposite polarity to the majority of vertices by π, followed by averaging the amplitudes of all vertices within a patch. The phase shifting prevents the vertices with opposite polarities from canceling each other out during the averaging operation.

2.6 Statistical analysis

Two-tailed non-parametric permutation tests were used to investigate differences in group means between the principal interactive *coupled* condition with all other behavioral conditions. In order to discern whether any differences were specific for the interaction itself, we also created surrogate data in the form of pseudo-pairs and compared with the real-pairs. A pseudo-pair is an artificial pair created by pairing the data from one participant with partners from all the other pairs except the real partner. Thus, we created $21 \times (21 - 1) = 420$ pseudo-pair surrogate data, which consisted of data from artificial pairs with individuals that both performed a given behavioral task; however, they were not time-locked to each other due to the lack of interaction (e.g., the observer from

one dyad was paired with the actor from another dyad). Multiple testing correction was performed using false discovery rate (FDR) and applied to each frequency range and feature type separately. The significant level was 0.05 for all hypothesis tests and the number of asterisks corresponded to different p-values ($^{*}p < 0.05$, $^{**}p < 0.01$, $^{***}p < 0.001$). Results are shown as mean with standard error of the mean (SEM).

3 Results

3.1 Interactive conditions were associated with greater behavioral synchrony

To evaluate the behavioral performances in the different conditions, we computed three movement features for each dyad and compared each condition with the principal interactive condition: the *coupled* condition. The asymmetric *observer-actor* (p-value $<$ 0.001) and *follower-leader* (p-value = 0.047) conditions exhibited a significantly greater difference in distance moved between the interacting participants compared to *coupled* condition, based on two-sided permutation tests with FDR multiple-comparison correction (Figure 1E). This difference indicates that the actor and leader moved their fingers more than the observer and follower, respectively. The interactive *coupled* condition displayed the greatest behavioral synchrony, evident by the high ratio of time the fingers of the dyads were in the same phase (Figure 1F) and high phase locking value (Figure 1G). The interactive *follower-leader* condition closely followed the *coupled* condition, with slightly lower in-phase ratio (Figure 1F; FDR corrected p-value = 0.029) and similar phase locking values (Figure 1G; FDR corrected p-value = 0.62). The non-social *control* condition was also associated with behavioral synchrony between the participants, due to the participants synchronizing to the same stimuli, albeit with a significantly lower in-phase ratio (Figure 1F; FDR corrected p-value $<$ 0.001) and phase locking value (Figure 1G; FDR corrected p-value = 0.033) compared to the *coupled* condition. Lastly, the *uncoupled* and *observer-actor* conditions displayed minimal behavioral synchrony, as expected (Figure 1F-G; FDR corrected p-values $<$ 0.001).

3.2 Single-brain microstate dynamics were not related to mirror-game conditions

Applying the microstate methodology to all the 42 individual single-brain EEG data, filtered in the alpha frequency range, yielded five microstates explaining around 56% of the variance (Figure 2A). The corresponding microstates determined in the beta and broadband frequency can be found in Supplementary Figure S1A and Supplementary Figure S2A, respectively. The topographies of the determined microstates estimated in the alpha, beta and broadband frequency range were very similar with each other (Supplementary Figure S3), and also qualitatively similar to the conventionally found resting-state EEG microstates in the literature (Michel and Koenig, 2018; Tarailis et al., 2023; Koenig et al., 2023). Thus we sorted and labeled the microstates in line with the prototypes from literature with microstate A showing a left-right orientation, B with a right-left orientation, C with an anterior-posterior orientation, D with a fronto-central maximum, and E with an occipito-central maximum (Férat et al., 2022; Tarailis et al., 2023; Koenig et al., 2023).

None of the computed alpha microstate features were related to the different behavioral conditions in the mirror-game, e.g. the ratio of time coverage of each of the five microstates was similar for all the different conditions (Figure 2B; lowest uncorrected p-value = 0.16, lowest FDR multiple test corrected p-value = 0.99, two-sided permutation test) and a similar result was also observed for the other microstate features: duration, occurrence, transition probabilities and entropy (Supplementary Figure S4, S5 and S8A), indicating no significant differences between any of the alpha microstate features across the conditions (lowest uncorrected p-value = 0.14, lowest FDR corrected p-value = 0.99). The same results were observed for the beta (Supplementary Figure S1, S6 and S8B; lowest uncorrected p-value = 0.015, lowest FDR corrected p-value = 0.76), and broadband frequency range (Supplementary Figure S2, S7 and S8C; lowest uncorrected p-value = 0.036, lowest FDR corrected p-value = 0.72) determined microstate features.

A high degree of correlations were found between the microstate features: duration, occurrence, transition probabilities and time coverage. For instance duration of microstate A is highly correlated with occurrence, transition probability and time coverage of microstate A, and the same holds

true for the other microstates (Supplementary Figure S9). For brevity, we focus the visualizations on time coverage (the other features can be found in the supplementary material).

3.3 Inter-brain co-occurrences of microstates were not related to mirror-game conditions

Estimation of inter-brain synchronization, defined as the co-occurrence of the same microstate at the same time point, also revealed no differences associated with the mirror-game conditions for time coverage of alpha microstates (Figure 3; lowest uncorrected p-value = 0.20, lowest FDR multiple test corrected p-value = 0.99, two-sided permutation tests). A similar result was also observed for the other alpha microstate features: duration, occurrence, transition probabilities and entropy with no significant associations between the inter-brain microstate features and mirror-game conditions (Supplementary Figure S10, S11 and S12A; lowest uncorrected p-value = 0.11, lowest FDR corrected p-value = 0.98). A lack of association between inter-brain microstate dynamics and mirror-game conditions were also observed for beta (Supplementary Figure S13, S14 and S12B; lowest uncorrected p-value = 0.02, lowest FDR corrected p-value = 0.86) and broadband microstate dynamics (Supplementary Figure S15, S16 and S12C; lowest uncorrected p-value = 0.06, lowest FDR corrected p-value = 0.98).

Surprisingly, the amount of time the two participants in a dyad were in the same microstate was not significant from chance-level for alpha, beta and broadband microstates (Supplementary Figure S17; lowest uncorrected p-value = 0.01, lowest FDR corrected p-value = 0.06). Allowing for a time-lag, i.e. shifting one of the microstate sequence time series relative to the other in a dyad of up to 1 second in both directions, only led to a negligible increase in the ratio of time the two participants' microstates were synchronized (less than 1%; Supplementary Figure S18). There was also no clear consistent time-lag where inter-brain synchronization peaked, reflected by the flat line when plotting ratio of time not in the same state and the time-lag (Supplementary Figure S19).

3.4 Two-brain microstate dynamics were different in the asymmetrical conditions

Due to the chance-level occurrence of similar global neuronal activity in the two participants in a dyad (either time-locked or time-shifted), we investigated a less constrained definition of inter-brain synchronization, by relaxing the constraint of being in the exact same microstate. This methodology is what we refer to as two-brain microstates, which tries to capture potentially different interpersonal neuronal activity states co-occurring over time in dyads.

Eight two-brain alpha microstates were determined when the microstate analysis was extended to be fitted on simultaneously recorded EEG from the 21 pairs (Figure 4A). Each two-brain microstate consists of a particular topography for one participant and a corresponding topography for the partner in the dyad at a specific time point. To distinguish them from single-brain microstates, we added a "d" (dual) prefix to their letter and a number to indicate the participant, e.g. dB1 refers to participant 1 dual-microstate B. The participant number is not so important for symmetric trials, but in the asymmetric trials we fixed the observer (in the observer-actor condition) or follower (in the follower-leader condition) to always be treated as participant 1 (top row in Figure 4A). Consequently the actor or leader was always treated as participant 2 (bottom row in Figure 4A). This was done to ensure that the effect of the asymmetric trials were not cancelled out by averaging across the asymmetry.

Remarkably, the two-brain alpha microstates were also very similar to the conventionally found single-brain resting-state EEG microstates, with dA1, dB1, dC1 and dD1 resembling our single-brain microstates A, B, C and E and dE2, dF2, dG2, dH2 and dC2 also resembling A, B, C, E and E, respectively. The rest of the topographies were more variable and not so clearly demarcated (Supplementary Figure S20A). Further investigation of the two-brain microstate topographies revealed that the absolute values for dA2, dB2, dC2 and dD2 were very close to 0, and similarly for dE1, dF1, dG1 and dH1 (Supplementary Figure S21A), indicating that these topographic maps reflect the arbitrary average neuronal activity. In other words, if a given time point is labeled as dA, dB, dC or dD, participant 1 has a global brain activity pattern corresponding to one of the four conventionally found resting-state microstates, while participant 2 has a non-specific brain activity pattern. The opposite is true for a time point labeled as dE, dF, dG and dH, with participant 2 in one of the conventionally found resting-state microstates, while participant 1 has a non-specific activity pattern.

Interestingly, the two-brain alpha microstate dynamics

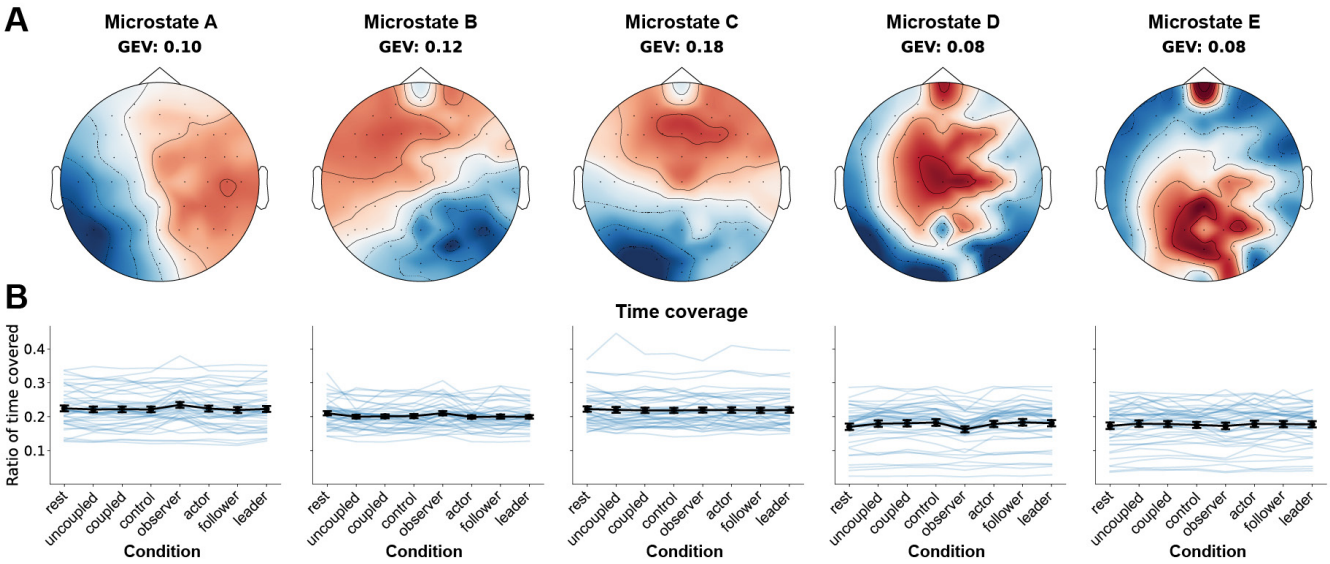

Fig. 2. **Conventional single-brain EEG microstate analysis.** A) Microstate analysis was performed on the 42 individual EEG timeseries filtered in the alpha frequency range and five microstates were determined, which explained around 56% of the variance. B) The ratio of time covered by each microstate was not related to the different behavioral conditions. GEV: global explained variance.

showed a clear difference in the asymmetrical trials compared to the symmetrical trials (Figure 4B). When compared to the principal symmetric condition, the *coupled* interaction, we observed that dA (p-value = 0.045) and dB (p-value = 0.008) were significantly higher and dE (p-value = 0.045), dF (p-value = 0.045) and dG (p-value = 0.040) were significantly lower for the *observer-actor* condition using two-sided permutation tests with FDR multiple-comparison correction. The same direction of changes (albeit not significant after multiple-comparison correction) were also observed for the *follower-leader* condition with a higher mean in dB (uncorrected p-value = 0.06, FDR corrected p-value = 0.304), dC (uncorrected p-value = 0.036, FDR corrected p-value = 0.208) and lower mean in dF (uncorrected p-value = 0.166, FDR corrected p-value = 0.554) and dG (uncorrected p-value = 0.126, FDR corrected p-value = 0.457). Significant differences in the *observer-actor* condition after multiple-comparison correction were also found for duration (Supplementary Figure S21B; lowest FDR corrected p-value = 0.008), occurrence (Supplementary Figure S21C; lowest FDR corrected p-value = 0.008), and transition probabilities (Supplementary Figure S22; lowest FDR corrected p-value = 0.013) in the alpha frequency range.

When the two-brain microstates were fitted in the beta frequency range (Supplementary Figure S23A), the determined microstates were also similar to the conventionally determined single-brain microstates, with dA1, dB1, dC1 and dD1 and dE2, dF2, dG2, dH2 resembling our single-brain microstates A, B, C and D for each participant, respectively (Supplementary Figure S20B). However, no differences in the two-brain beta microstate features were observed for the different behavioral conditions (Supplementary Figure S23B-D and S24; lowest uncorrected p-value = 0.04, lowest FDR corrected p-value = 0.97).

Similar results were observed for two-brain microstates fitted in the broadband frequency range (Supplementary Figure S25A), with topographies resembling single-brain microstate topographies for each participant respectively (Supplementary Figure S20C), but no differences associated with the different behavioral conditions (Supplementary Figure S25B-D and S26; lowest uncorrected p-value = 0.02, lowest FDR corrected p-value = 0.83).

In order to discern whether the changes in two-brain alpha microstate dynamics were specific to the interaction itself, as opposed to an effect of the asymmetrical behavioral assignment, we computed the microstate features for pseudo-pairs. We observed that the pseudo-pairs also showed a significant difference in two-brain microstate dynamics for the asymmet-

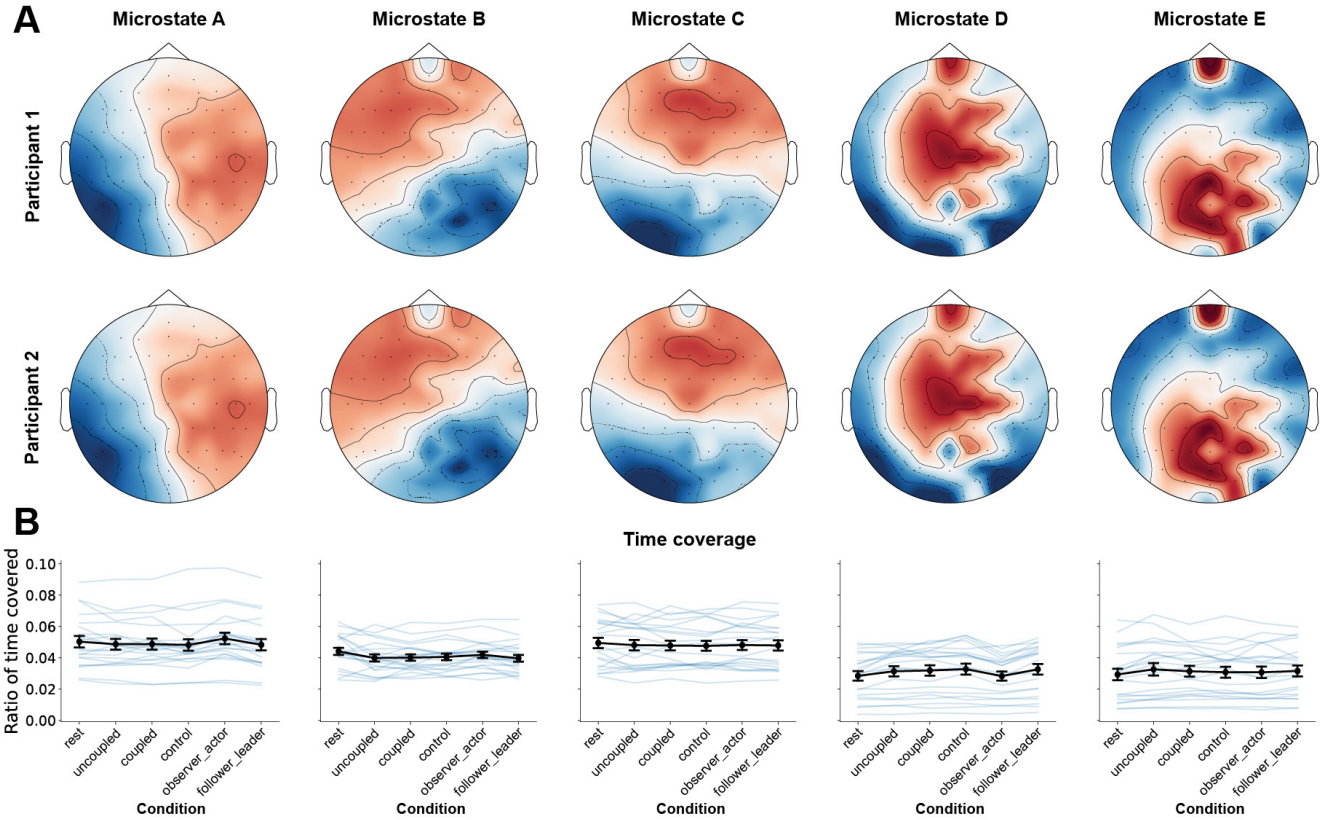

Fig. 3. **Inter-brain synchronization of microstates.** A) We investigated the co-occurrence of similar microstates in the two participants in the dyads performing the mirror-game. B) The ratio of time the participants were in the same microstate was not related to the different behavioral conditions. The ratio of time coverage was normalized to the total time they were in the same microstate and the time not in the same microstate (Supplementary Figure S17), hence the low values.

rical tasks, and there was no difference in time coverage between the real pairs and the pseudo-pairs (Supplementary Figure S27A; lowest uncorrected p-value = 0.734, lowest FDR corrected p-value = 0.994). The lack of difference was also observed in duration, occurrence and transition probabilities (lowest uncorrected p-value = 0.349, lowest FDR corrected p-value = 0.997) suggesting that the changes in two-brain alpha microstate dynamics were not specific to the interaction, but rather the asymmetrical task.

3.5 Two-brain microstate complexity features were not related to mirror-game conditions

We also estimated two features pertaining to the complexity of the microstates: entropy and long-range temporal correlations (von Wegner et al., 2023) for two-brain microstates. Entropy was computed as Shannon entropy and long-range temporal correlations were estimated using DFA. We did not observe any differences in microstate entropy between the mirror-game tasks for any of the three frequency ranges investigated (Supplementary Figure S28A-C; lowest uncorrected p-value = 0.34, lowest FDR corrected p-value = 0.93). There were also no differences in entropy between real and pseudo-pairs (Supplementary Figure S27B; lowest uncorrected p-value = 0.771, lowest FDR corrected p-value = 0.900)

To perform the DFA analysis, the microstate sequence time series had to be partitioned into two classes (Van De Ville et al., 2010), and given the asymmetric topographies with dA, dB, dC and dD reflecting participant 1 being in a conventional resting-state microstate, and dE, dF, dG and dH reflecting participant 2, respectively, we partitioned the two classes as $C_1 = \{dA, dB, dC, dD\}, C_2 = \{dE, dF, dG, dH\}$. We observed that the *rest* condition was significantly different from the *coupled* condition, for all three frequency ranges, while

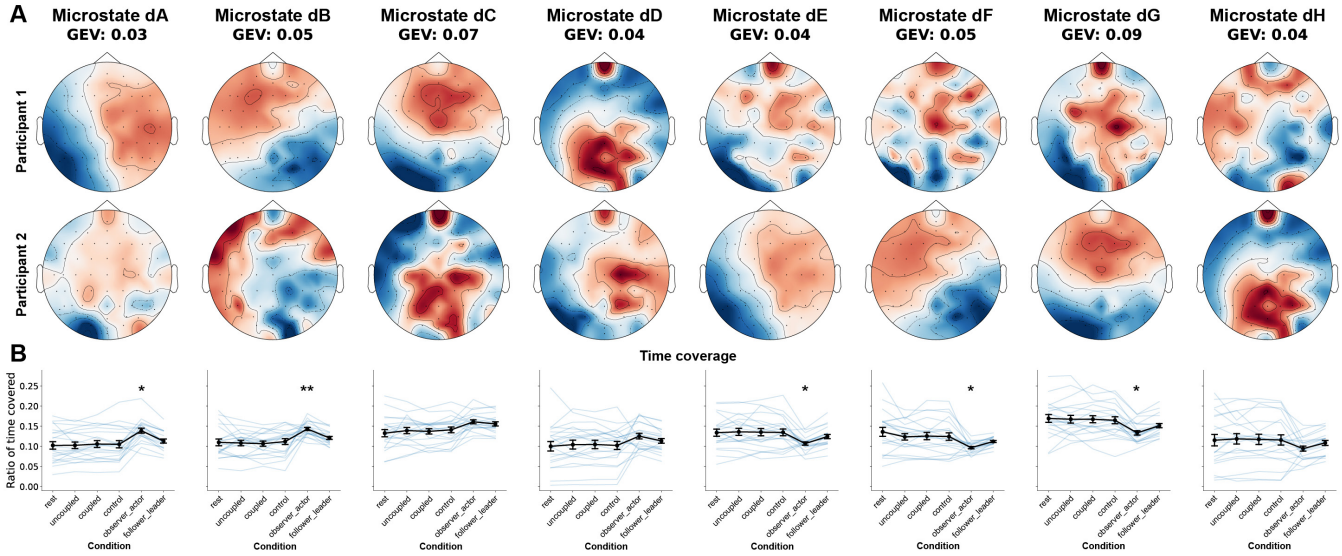

Fig. 4. **Two-brain EEG microstate analysis.** A) Microstate analysis was performed on the simultaneously recorded EEG from 21 pairs collected during the mirror-game paradigm, which yielded eight two-brain alpha microstates, explaining around 41% of the variance. B) The ratio of time covered by each two-brain microstate was different between the asymmetrical and symmetrical conditions, with only the observer-actor condition differing after multiple-comparison correction. GEV: global explained variance.

the *uncoupled* condition was also different in the beta and broadband frequency band and *control* and *observer-actor* condition was different from *coupled* in the beta frequency band (Supplementary Figure S28D-F; all FDR corrected p-values < 0.01). None of the other conditions were significantly different. There were also no differences in DFA exponents between real and pseudo-pairs (Supplementary Figure S27C; lowest uncorrected p-value = 0.392, lowest FDR corrected p-value = 0.796).

3.6 Source localization of two-brain microstates

To determine the underlying cortical neural sources for each two-brain microstate, we applied eLORETA to the microstate topographies. Due to the high similarities between the topographies obtained from the three frequency ranges, only the two-brain alpha microstates are shown (Figure 5). We observed that the cortical neural sources corresponding to the four conventionally found resting-state microstates were similar between the two participants in a pair. Focusing on the areas with greatest activity, we observed that dA1 and dE2 showed high activity in left temporal and parietal areas and low activity in left temporal and right cingulate and parietal areas (Figure 6A and 6E). dB1 and dF2 showed high activity in right parietal, temporal and cingulate areas and low activity in right temporal and left cingulate areas (Figure 6B and 6F). dC1 and dG2 showed high activity in left cingulate and temporal areas and low activity in Left and right temporal areas (Figure 6C and 6G). dD1 and dH2 showed high activity in left and right frontal and left anterior cingulate areas and low activity in left occipital areas (Figure 6D and 6H). Notice that due to the microstate polarity invariance during the clustering, the high and low activity labels are arbitrary and interchangeable. The keypoint is that there is a difference in potential between the areas listed in high and low. Additionally, the microstates reflecting the arbitrary mean neuronal activity (dA2, dB2, dC2, dD2, dE1, dF1, dG1 and dH1) were omitted as their corresponding source activities were also around 0. For readers unfamiliar with flatmaps, Supplementary Figure S29 shows the underlying sources with the more standard view of the cortical regions on the inflated brain.

4 Discussion

In this study, we developed a novel method for investigating inter-brain synchronization and inter-brain asymmetry in a hyperscanning EEG experiment. Specifically, we expanded the microstate analysis framework to dyads of interacting participants, enabling us to investigate quasi-stable moments

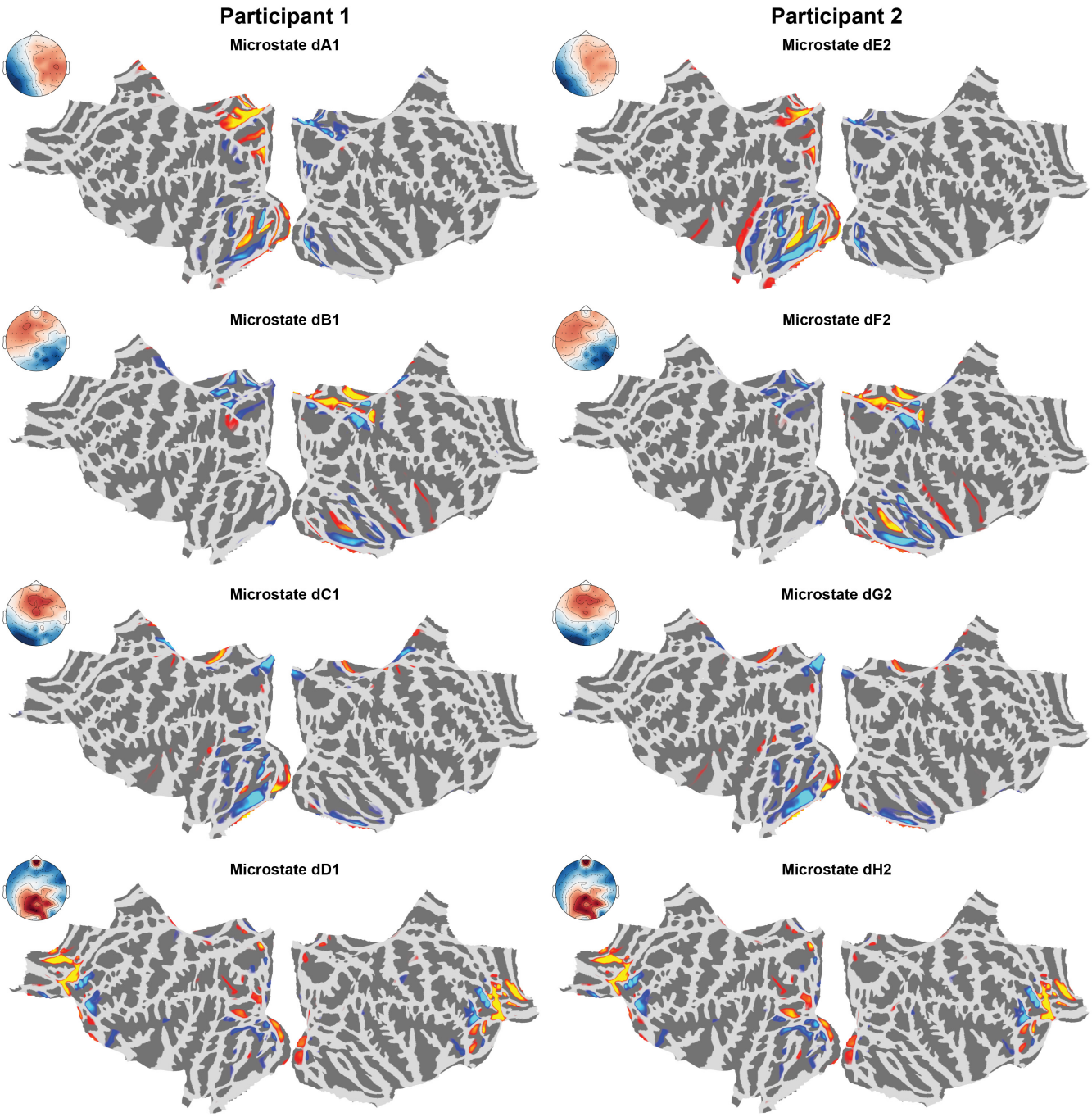

Fig. 5. **The eight two-brain alpha microstates and their corresponding eLORETA cortical activities.** We only show the cortical sources for dA1, dB1, dC1, dD1, dE2, dF2, dG2 and dH2, as the other two-brain microstates reflected the mean arbitrary activity. See Supplementary Figure S29 for the same data plotted with an inflated brain view.

of synchronized, as well as asymmetric inter-brain activity. We found that conventional microstates fitted to individuals (single-brain microstates) were not related to the different task conditions; however, the dynamics of the two-brain alpha microstates were changed for the *observer-actor* condition, compared to all other conditions where participants had more symmetric task demands (rest, individual, joint). Interestingly, the topographies of the two-brain microstates

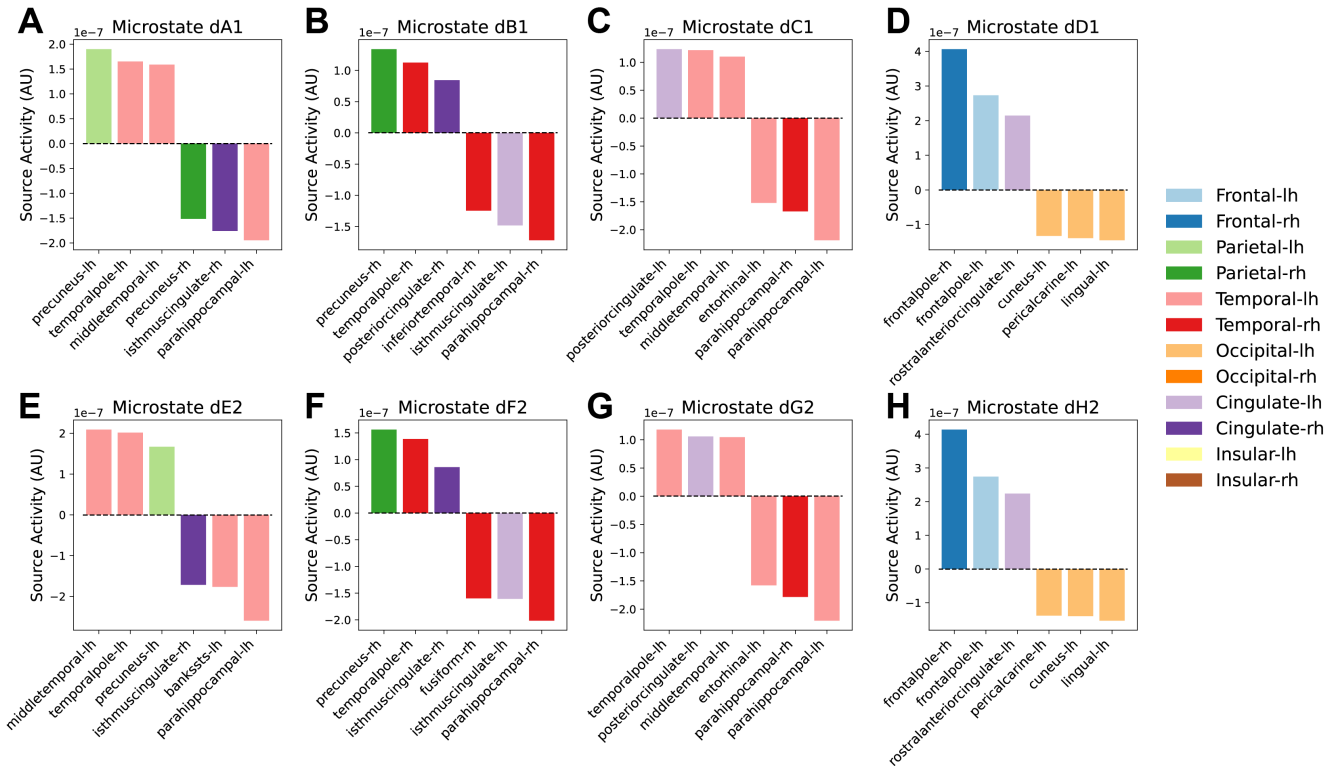

Fig. 6. **Top three positive and negative areas in the eight source localized two-brain alpha microstates.** The colors indicate which brain region the corresponding area belong to, while the shade indicate whether it is the left or high hemisphere, with darker colors belonging to the right hemisphere. The dashed black line indicates zero activity. Notice that due to the microstate polarity invariance during clustering, the positive or negative activity signs are interchangeable.

were related to the conventionally found resting-state microstates determined from single individuals (Tarailis et al., 2023), and our source localized two-brain microstates (Figure 5) also had cortical activities similar to previous findings relating the microstates to the Default Mode Network (DMN) (Pascual-Marqui et al., 2014).

One often discussed topic regarding microstate analysis is the frequency range of the data the clustering should be fitted to. In the early microstate papers, the alpha frequency range was employed (Lehmann et al., 1987), but later papers found that the resting-state microstates could also be determined using broadband, e.g. 2-20 Hz or 1-40 Hz, which has subsequently become the more standard approach (Tarailis et al., 2023). However, alpha oscillations are regarded as the main driving component for broadband microstates (Milz et al., 2017; von Wegner et al., 2021). As our EEG data were not only from a resting-state condition, but recorded during an interactive mirror-game paradigm where the participants were producing motor movements, we were also interested in the beta frequency range (13-30Hz), which is known to be important for motor movements (Conway et al., 1995; Perez et al., 2006; Baker, 2007). A recent paper (Férat et al., 2022) also demonstrated that despite the near-perfect spatial correlations between microstate topographies across frequencies for both eyes open and eyes closed at rest, spectrally specific microstate analysis yielded independent information about spatial-temporal dynamics, with alpha-band microstates classifying eyes open from eyes closed EEG better than broadband microstate features (Férat et al., 2022). Therefore, we performed the microstate analysis for all three frequency ranges of interest in parallel. Consistent with previous results (Férat et al., 2022) the topographies of our determined single-brain microstates were very similar across frequency ranges, and we also showed that two-brain microstates were similar across frequencies. However, we only found significant differences associated with the asymmetric *observer-actor*

condition in the alpha frequency range for the two-brain microstates. Previous studies have also found associations between alpha/mu oscillations and motor control, joint attention, and coordination (Klimesch et al., 2007; Tognoli et al., 2007; Lachat et al., 2012; Dumas et al., 2012), e.g., showing role-specific modulation of alpha-band activity when participants lead or follow (Konvalinka et al., 2014; Flösch et al., 2023) or when different interpersonal strategies emerge (Heggli et al., 2021). Our findings showing that two-brain alpha microstates were specifically associated with differences during the asymmetric tasks is also consistent with the recent hyperscanning dual EEG findings by Flösch et al. (2023), who found differences in alpha and low beta oscillations over large areas (frontal, central and parietal areas) in dyads performing a cooperative task with asymmetric roles (sender and receiver).

The functional role of our findings is still unclear and further investigation is needed to better understand the neural mechanisms. However the cortical areas associated with our determined microstates have been postulated to be a fragmented high time resolution version of the slow metabolically (PET/fMRI) determined Default Mode Network (DMN) (Pascual-Marqui et al., 2014). Given the similar trends with higher presence of dA, dB, dC and dD in the observer and lower presence of dE, dF, dG and dH in the actor, we hypothesize that the effect we observe is due to the observer being in a more resting-state DMN-like neuronal brain state compared to the actor. Importantly, this effect is only observed for the two-brain microstates and not found for single-brain microstates, indicating that both participants in the dyads have DMN activity; however the relative degree of activity might not be equal, and this difference can only be determined when analysing both participants simultaneously. An important point about two-brain microstates is that one time point is always associated with only one label, hence if the label is dA, then it means participant 1 is more in a resting-state A microstate than participant 2. They are competing for label assignment, whereas in single-brain microstates they both get assigned a microstate for each time step, thus there is no competition or comparison between the individuals. The difference we observed between the symmetric interactive *coupled* condition and *observer-actor* condition could thus correspond to the DMN being more active in the observer relative to the actor, compared to the symmetrical trials where the DMNs are equally active.

Another discussed topic regarding microstate analysis and unsupervised clustering is the number of clusters that should be extracted. Too few might not capture enough information about the data; however, too many clusters could lead to overfitting, which result in the clusters not being able to generalize. There are various methods to determine an optimal number of microstates and it is also possible to use several methods in combination, e.g. the meta-criterion (Custo et al., 2017). We used the cross-validation criterion (Pascual-Marqui et al., 1995) and found five and eight microstates to be optimal for the single-brain and two-brain analysis, respectively. One might argue that one reason for not finding any task-related differences in single-brain microstates could be due to the lower number of extracted microstates, and subsequently lesser information captured. However, the fact that the topographies of the two-brain microstates show high similarity to four of the single-brain microstates, provides some evidence that they are not capturing less information. Additionally, the global explained variance was higher for the single-brain microstates compared to two-brain microstates, most likely due to the concatenated two-brain EEG time-series being more variable and thus harder to reduce into specific quasi-stable states. To fully resolve this issue, we also repeated the single-brain microstate analysis with eight clusters and we still did not observe any task-related differences in microstate dynamics (Supplementary Figure S30). Noticeably, the global explained variance only increased with 4% by adding three more microstates, emphasizing the point that once too many clusters are added, the clusters might begin to overfit and only fit to smaller (potentially noisy) portions of the data.

The oscillatory nature of neural activity of EEG is also one of the reasons why the K-means algorithm had to be modified to be polarity invariant for the determination of microstates (Pascual-Marqui et al., 1995). One of the challenges of expanding the microstate analysis from single individuals to dyads was to retain the polarity invariance for both individuals in a pair. The standard implementation to ignore polarity in microstates is to square the spatial correlation coefficient (von Wegner et al., 2021). But this solution does not ensure that the individual topographies from each participant

in a two-brain microstate were polarity invariant. For example in the case of dA1 and dA2: if we define them as having a positive polarity, then the topographies can be written as {+, +}. If the microstates are polarity invariant, the following polarities should be equivalent: {+, +}, {+, -}, {-, +} and {-, -}. However, using the squared spatial correlation coefficient only ensures {+, +} will be treated the same as {-, -}, but a neural activity pattern similar to {+, -} or {-, +} would not be equivalent. Another method to make microstates polarity invariant is to use the absolute transformation (Tait and Zhang, 2022). Initially, we also tried the absolute transformation, and while the microstates were polarity invariant, there is a large caveat with this method, namely that negative and positive values will be treated equally, and this fundamentally changes the data, e.g. if Fp1 is 20µV, Fp2 is 16µV, O1 is -19µV and O2 is -21µV, then after the absolute transformation Fp1 would be seen as more similar to O1 and O2 as opposed to Fp2. Such a dramatic change of the data would also change what kind of microstates will be determined. Ultimately, we decided to compute the spatial correlation for each time point with all four combinations of possible polarity configurations, and chose to keep the highest correlation, to preserve the polarity invariance for the microstate determination, without compromising the input data.

Remarkably, both the single-brain and two-brain microstate topographies were similar to the commonly found resting-state EEG microstates in previous literature (Michel and Koenig, 2018; Tarailis et al., 2023), despite being extracted from the motor coordination tasks during the mirror-game. One reason for this similarity could have been due to the presence of the 2min rest condition at the start and end of the experiment. To address this, we also tried fitting the two-brain microstates without the *rest* conditions and observed similar two-brain microstates (Supplementary Figure S31), indicating that the reason for the similarity to the commonly found resting-state single-brain EEG microstates was not due to being fitted on rest conditions.

It has not escaped our notice, that we were not able to find inter-brain synchronization, either as simultaneous occurrence of inter-brain microstates, or as quasi-stable co-occurring brain-states in the dyads. In fact, the amount of time the two participants were in the same microstate was not different from chance-level (Supplementary Figure S17). Importantly, the determined two-brain microstates, which are optimized to explain as much of the variance in the data as possible, all corresponded to a stable canonical microstate in one participant, while the other participant had activity close to 0 and hence corresponded to arbitrary undetermined activity. This does not mean that there was not any inter-brain synchronization during behavioural synchronization or interaction, as the microstates only focus on global neuronal brain states, hence smaller spatially focal synchronized areas would be overlooked by this methodology. It would be interesting for future work to investigate comparisons between focal interbrain synchronization (e.g. utilizing phase locking value or circular correlations (Zamm et al., 2024)) and global brain state synchronization using microstates.

5 Conclusion

Taken together, two-brain microstates might serve as a novel method for identifying both synchronized and asymmetric inter-brain states during real-time social interaction. In this study, we show that two-brain microstates are modulated by asymmetric interactions, which are not driven by the interaction itself but by the asymmetry in the tasks. To further validate the method, future work should apply the methodology to other behavioral tasks where asymmetric behaviour is both intentional (instructed) as well as spontaneous. In addition, the methodology has an added benefit of being expandable, thus multi-brain microstates could be utilized to investigate neural mechanisms underlying social interaction in groups of people.

Data and code availability

The raw EEG data that support the findings of this study are openly available (Zimmermann et al., 2022) from Figshare at https://figshare.com/s/5e3dcb56ed515c2cb786.

The code used for this study is available from https://lab.compute.dtu.dk/glia/two-brain-eeg-analysis.

CRediT authorship contribution statement

Q.L.: conceptualization, methodology, software, formal analysis, data curation, visualization, project administration, writing-original draft and writing-review and editing; M.Z.: software, investigation, data curation, writing-review and editing; I.K.: conceptualization, investigation, resources,

supervision, funding acquisition, writing—original draft and writing—review and editing. All authors approved the final version of the manuscript.

Declaration of Competing Interests

The authors take full responsibility for the content of the publication. We declare we have no competing interests.

Acknowledgements

This work is supported by the Villum Young Investigator grant (project no. 37525).

References

Ahn, S., Cho, H., Kwon, M., Kim, K., Kwon, H., Kim, B. S., Chang, W. S., Chang, J. W., and Jun, S. C. (2018). Interbrain phase synchronization during turn-taking verbal interaction—a hyperscanning study using simultaneous EEG/MEG. *Human Brain Mapping*, 39(1):171–188. _eprint: https://onlinelibrary.wiley.com/doi/pdf/10.1002/hbm.23834.

Astolfi, L., Toppi, J., De Vico Fallani, F., Vecchiato, G., Salinari, S., Mattia, D., Cincotti, F., and Babiloni, F. (2010). Neuroelectrical hyperscanning measures simultaneous brain activity in humans. *Brain Topography*, 23(3):243–256. Publisher: Springer.

Ayrolles, A., Brun, F., Chen, P., Djalovski, A., Beauxis, Y., Delorme, R., Bourgeron, T., Dikker, S., and Dumas, G. (2021). HyPyP: a Hyperscanning Python Pipeline for interbrain connectivity analysis. *Social Cognitive and Affective Neuroscience*, 16(1-2):72–83.

Babiloni, F. and Astolfi, L. (2014). Social neuroscience and hyperscanning techniques: Past, present and future. *Neuroscience & Biobehavioral Reviews*, 44:76–93.

Babiloni, F., Cincotti, F., Mattia, D., De Vico Fallani, F., Tocci, A., Bianchi, L., Salinari, S., Marciani, M., Colosimo, A., and Astolfi, L. (2007). High Resolution EEG Hyperscanning During a Card Game. In *2007 29th Annual International Conference of the IEEE Engineering in Medicine and Biology Society*, pages 4957–4960, Lyon, France. IEEE. ISSN: 1557-170X.

Baccalá, L. A. and Sameshima, K. (2001). Partial directed coherence: A new concept in neural structure determination. *Biological Cybernetics*, 84(6):463–474.

Baker, S. N. (2007). Oscillatory interactions between sensorimotor cortex and the periphery. *Current Opinion in Neurobiology*, 17(6):649–655. Publisher: Elsevier Ltd ISBN: 0959-4388 (Print) 0959-4388 (Linking).

Conway, B. a., Halliday, D. M., Farmer, S. F., Shahani, U., Maas, P., Weir, a. I., and Rosenberg, J. R. (1995). Synchronization between motor cortex and spinal motoneuronal pool during the performance of a maintained motor task in man. *The Journal of physiology*, 489(3):917–924. ISBN: 0022-3751 (Print) 0022-3751 (Linking).

Cui, X., Bryant, D. M., and Reiss, A. L. (2012). NIRS-based hyperscanning reveals increased interpersonal coherence in superior frontal cortex during cooperation. *NeuroImage*, 59(3):2430–2437.

Custo, A., Van De Ville, D., Wells, W. M., Tomescu, M. I., Brunet, D., and Michel, C. M. (2017). Electroencephalographic Resting-State Networks: Source Localization of Microstates. *Brain Connectivity*, 7(10):671–682. Publisher: Mary Ann Liebert, Inc., publishers.

Czeszumski, A., Eustergerling, S., Lang, A., Menrath, D., Gerstenberger, M., Schuberth, S., Schreiber, F., Rendon, Z. Z., and König, P. (2020). Hyperscanning: A Valid Method to Study Neural Inter-brain Underpinnings of Social Interaction. *Frontiers in Human Neuroscience*, 14.

De Jaegher, H., Di Paolo, E., and Gallagher, S. (2010). Can social interaction constitute social cognition? *Trends in Cognitive Sciences*, 14(10):441–447.

Dingemanse, M., Liesenfeld, A., Rasenberg, M., Albert, S., Ameka, F. K., Birhane, A., Bolis, D., Cassell, J., Clift, R., Cuffari, E., De Jaegher, H., Novaes, C. D., Enfield, N. J., Fusaroli, R., Gregoromichelaki, E., Hutchins, E., Konvalinka, I., Milton, D., Raczaszek-Leonardi, J., Reddy, V., Rossano, F., Schlangen, D., Seibt, J., Stokoe, E., Suchman, L., Vesper, C., Wheatley, T., and Wiltschko, M. (2023). Beyond Single-Mindedness: A Figure-Ground Reversal for the Cognitive Sci-

ences. *Cognitive Science*, 47(1):e13230. _eprint: https://onlinelibrary.wiley.com/doi/pdf/10.1111/cogs.13230.

Dumas, G. (2011). Towards a two-body neuroscience. *Communicative & Integrative Biology*, 4(3):349–352.

Dumas, G., Martinerie, J., Soussignan, R., and Nadel, J. (2012). Does the brain know who is at the origin of what in an imitative interaction? *Frontiers in Human Neuroscience*, 6.

Dumas, G., Nadel, J., Soussignan, R., Martinerie, J., and Garnero, L. (2010). Inter-Brain Synchronization during Social Interaction. *PLOS ONE*, 5(8):e12166. Publisher: Public Library of Science.

Fischl, B. (2012). FreeSurfer. *NeuroImage*, 62(2):774–781.

Flösch, K.-P., Flaisch, T., Imhof, M. A., and Schupp, H. T. (2023). Alpha/beta oscillations reveal cognitive and affective brain states associated with role taking in a dyadic cooperative game. *Cerebral Cortex*, page bhad487.

Férat, V., Seeber, M., Michel, C. M., and Ros, T. (2022). Beyond broadband: Towards a spectral decomposition of electroencephalography microstates. *Human Brain Mapping*, 43(10):3047–3061. _eprint: https://onlinelibrary.wiley.com/doi/pdf/10.1002/hbm.25834.

Gramfort, A., Luessi, M., Larson, E., Engemann, D. A., Strohmeier, D., Brodbeck, C., Goj, R., Jas, M., Brooks, T., Parkkonen, L., and Hämäläinen, M. (2013). MEG and EEG data analysis with MNE-Python. *Frontiers in Neuroscience*, 7:1–13.

Hamilton, A. F. d. C. (2021). Hyperscanning: Beyond the Hype. *Neuron*, 109(3):404–407.

Hardstone, R., Poil, S. S., Schiavone, G., Jansen, R., Nikulin, V. V., Mansvelder, H. D., and Linkenkaer-Hansen, K. (2012). Detrended fluctuation analysis: A scale-free view on neuronal oscillations. *Frontiers in Physiology*, pages 1–13.

Heggli, O. A., Konvalinka, I., Cabral, J., Brattico, E., Kringelbach, M. L., and Vuust, P. (2021). Transient brain networks underlying interpersonal strategies during synchronized action. *Social Cognitive and Affective Neuroscience*, 16(Jan):19–30.

Holroyd, C. B. (2022). Interbrain synchrony: on wavy ground. *Trends in Neurosciences*, 45(5):346–357. Publisher: Elsevier.

Hu, Y., Pan, Y., Shi, X., Cai, Q., Li, X., and Cheng, X. (2018). Inter-brain synchrony and cooperation context in interactive decision making. *Biological Psychology*, 133:54–62.

Klimesch, W., Sauseng, P., and Hanslmayr, S. (2007). EEG alpha oscillations: The inhibition-timing hypothesis. *Brain Research Reviews*, 53(1):63–88. Publisher: Elsevier.

Koenig, T., Diezig, S., Kalburgi, S. N., Antonova, E., Artoni, F., Brechet, L., Britz, J., Croce, P., Custo, A., Damborská, A., Deolindo, C., Heinrichs, M., Kleinert, T., Liang, Z., Murphy, M. M., Nash, K., Nehaniv, C., Schiller, B., Smailovic, U., Tarailis, P., Tomescu, M., Toplutaş, E., Vellante, F., Zanesco, A., Zappasodi, F., Zou, Q., and Michel, C. M. (2023). EEG-Meta-Microstates: Towards a More Objective Use of Resting-State EEG Microstate Findings Across Studies. *Brain Topography*.

Konvalinka, I., Bauer, M., Stahlhut, C., Hansen, L. K., Roepstorff, A., and Frith, C. D. (2014). Frontal alpha oscillations distinguish leaders from followers: Multivariate decoding of mutually interacting brains. *NeuroImage*, 94:79–88.

Konvalinka, I., Kompatsiari, K., and Li, Q. (2023). The fine-grained temporal dynamics of social timing: a window into sociality of embodied social agents. Comment on "The evolution of social timing" by L. Verga, S. A. Kotz, & A. Ravignani. *Physics of Life Reviews*, 47:95–98.

Konvalinka, I. and Roepstorff, A. (2012). The two-brain approach: how can mutually interacting brains teach us something about social interaction? *Frontiers in Human Neuroscience*, 6.

Koul, A., Ahmar, D., Iannetti, G. D., and Novembre, G. (2023). Spontaneous dyadic behavior predicts the emergence of interpersonal neural synchrony. *NeuroImage*, 277:120233.

Lachat, F., hugeville, l., lemarechal, j.-d., conty, l., and George, N. (2012). Oscillatory Brain Correlates of Live Joint Attention: A Dual-EEG Study. *Frontiers in Human Neuroscience*, 6.

Lachaux, J. P., Rodriguez, E., Martinerie, J., and Varela, F. J. (1999). Measuring phase synchrony in brain signals. *Human Brain Mapping*, 8(4):194–208.

Lehmann, D., Ozaki, H., and Pal, I. (1987). EEG alpha map series: brain micro-states by space-oriented adaptive segmentation. *Electroencephalography and Clinical Neurophysiology*, 67(3):271–288.

Lindenberger, U., Li, S.-C., Gruber, W., and Müller, V. (2009). Brains swinging in concert: cortical phase synchronization while playing guitar. *BMC Neuroscience*, 10(1):22.

Michel, C. M. and Koenig, T. (2018). EEG microstates as a tool for studying the temporal dynamics of whole-brain neuronal networks: A review. *NeuroImage*, 180:577–593. Publisher: Academic Press.

Milz, P., Pascual-Marqui, R. D., Achermann, P., Kochi, K., and Faber, P. L. (2017). The EEG microstate topography is predominantly determined by intracortical sources in the alpha band. *NeuroImage*, 162:353–361. Publisher: Academic Press.

Montague, P. R., Berns, G. S., Cohen, J. D., McClure, S. M., Pagnoni, G., Dhamala, M., Wiest, M. C., Karpov, I., King, R. D., Apple, N., and Fisher, R. E. (2002). Hyperscanning: Simultaneous fMRI during Linked Social Interactions. *NeuroImage*, 16(4):1159–1164.

Noy, L., Dekel, E., and Alon, U. (2011). The mirror game as a paradigm for studying the dynamics of two people improvising motion together. *Proceedings of the National Academy of Sciences of the United States of America*, 108(52):20947–20952. Publisher: National Academy of Sciences.

Pascual-Marqui, R. D., Lehmann, D., Faber, P., Milz, P., Kochi, K., Yoshimura, M., Nishida, K., Isotani, T., and Kinoshita, T. (2014). The resting microstate networks (RMN): cortical distributions, dynamics, and frequency specific information flow. arXiv:1411.1949 [q-bio].

Pascual-Marqui, R. D., Michel, C. M., and Lehmann, D. (1995). Segmentation of Brain Electrical Activity into Microstates; Model Estimation and Validation. *IEEE Transactions on Biomedical Engineering*, 42(7):658–665.

Perez, M. A., Lundbye-Jensen, J., and Nielsen, J. B. (2006). Changes in corticospinal drive to spinal motoneurones following visuo-motor skill learning in humans. *The Journal of Physiology*, 573(3):843–855. ISBN: 0022-3751 (Print)\r0022-3751 (Linking).

Schilbach, L., Timmermans, B., Reddy, V., Costall, A., Bente, G., Schlicht, T., and Vogeley, K. (2013). Toward a second-person neuroscience. *Behavioral and Brain Sciences*, 36(4):393–414.

Sebanz, N., Bekkering, H., and Knoblich, G. (2006). Joint action: Bodies and minds moving together. *Trends in Cognitive Sciences*, 10(2):70–76. Publisher: Elsevier Current Trends.

Tait, L. and Zhang, J. (2022). MEG cortical microstates: Spatiotemporal characteristics, dynamic functional connectivity and stimulus-evoked responses. *NeuroImage*, 251:119006.

Tarailis, P., Koenig, T., Michel, C. M., and Griškova-Bulanova, I. (2023). The Functional Aspects of Resting EEG Microstates: A Systematic Review. *Brain Topography*.

Tognoli, E., Lagarde, J., DeGuzman, G. C., and Kelso, J. A. S. (2007). The phi complex as a neuromarker of human social coordination. *Proceedings of the National Academy of Sciences*, 104(19):8190–8195. Publisher: Proceedings of the National Academy of Sciences.

Van De Ville, D., Britz, J., and Michel, C. M. (2010). EEG microstate sequences in healthy humans at rest reveal scale-free dynamics. *Proceedings of the National Academy of Sciences*, 107(42):18179–18184. Publisher: Proceedings of the National Academy of Sciences.

von Wegner, F., Bauer, S., Rosenow, F., Triesch, J., and Laufs, H. (2021). EEG microstate periodicity explained by rotating phase patterns of resting-state alpha oscillations. *NeuroImage*, 224:117372.

von Wegner, F. and Laufs, H. (2018). Information-theoretical analysis of EEG microstate sequences in python. *Frontiers in Neuroinformatics*, 12(June):1–10.

von Wegner, F., Wiemers, M., Hermann, G., Tödt, I., Tagliazucchi, E., and Laufs, H. (2023). Complexity Measures for EEG Microstate Sequences: Concepts and Algorithms. *Brain Topography*.

Zamm, A., Debener, S., Bauer, A.-K. R., Bleichner, M. G., Demos, A. P., and Palmer, C. (2018). Amplitude envelope correlations measure synchronous cortical oscillations in performing musicians. *Annals of the New York Academy of Sciences*, 1423(1):251–263. _eprint: https://onlinelibrary.wiley.com/doi/pdf/10.1111/nyas.13738.

Zamm, A., Loehr, J. D., Vesper, C., Konvalinka, I., Kappel, S. L., Heggli, O. A., Vuust, P., and Keller, P. E. (2024). A Practical Guide to EEG Hyperscanning in Joint Action Research: From Motivation to Implementation. *Social Cognitive and Affective Neuroscience*, 19(1). Publisher: PsyArXiv.

Zimmermann, M., Lomoriello, A. S., and Konvalinka, I. (2022). Intra-individual behavioural and neural signatures of audience effects and interactions in a mirror-game paradigm. *Royal Society Open Science*, 9(2). Publisher: The Royal Society.

Zimmermann, M., Schultz-Nielsen, K., Dumas, G., and Konvalinka, I. (2024). Arbitrary methodological decisions skew inter-brain synchronization estimates in hyperscanning-EEG studies. Publisher: OSF.

Supplementary Materials

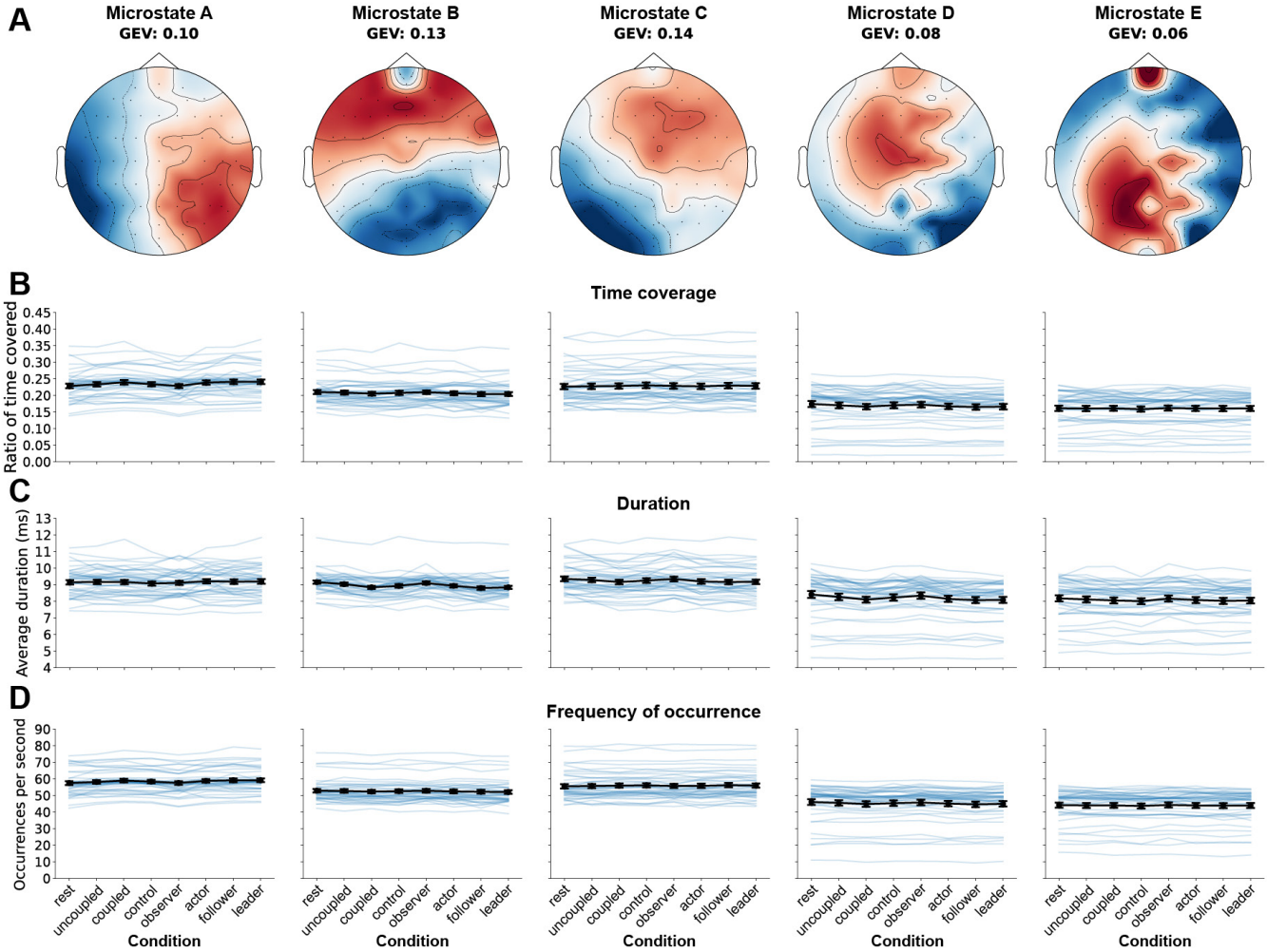

Fig. S1. **Conventional single-brain EEG beta microstate analysis.** A) Microstate analysis was performed on the 42 individual EEG timeseries filtered in the beta frequency range and five microstates were determined, which explained around 50% of the variance. B) The ratio of time covered of each microstate. C) The average duration of each microstate. D) The frequency of occurrence for each microstate. None of the features were related to the different behavioral conditions. GEV: global explained variance.

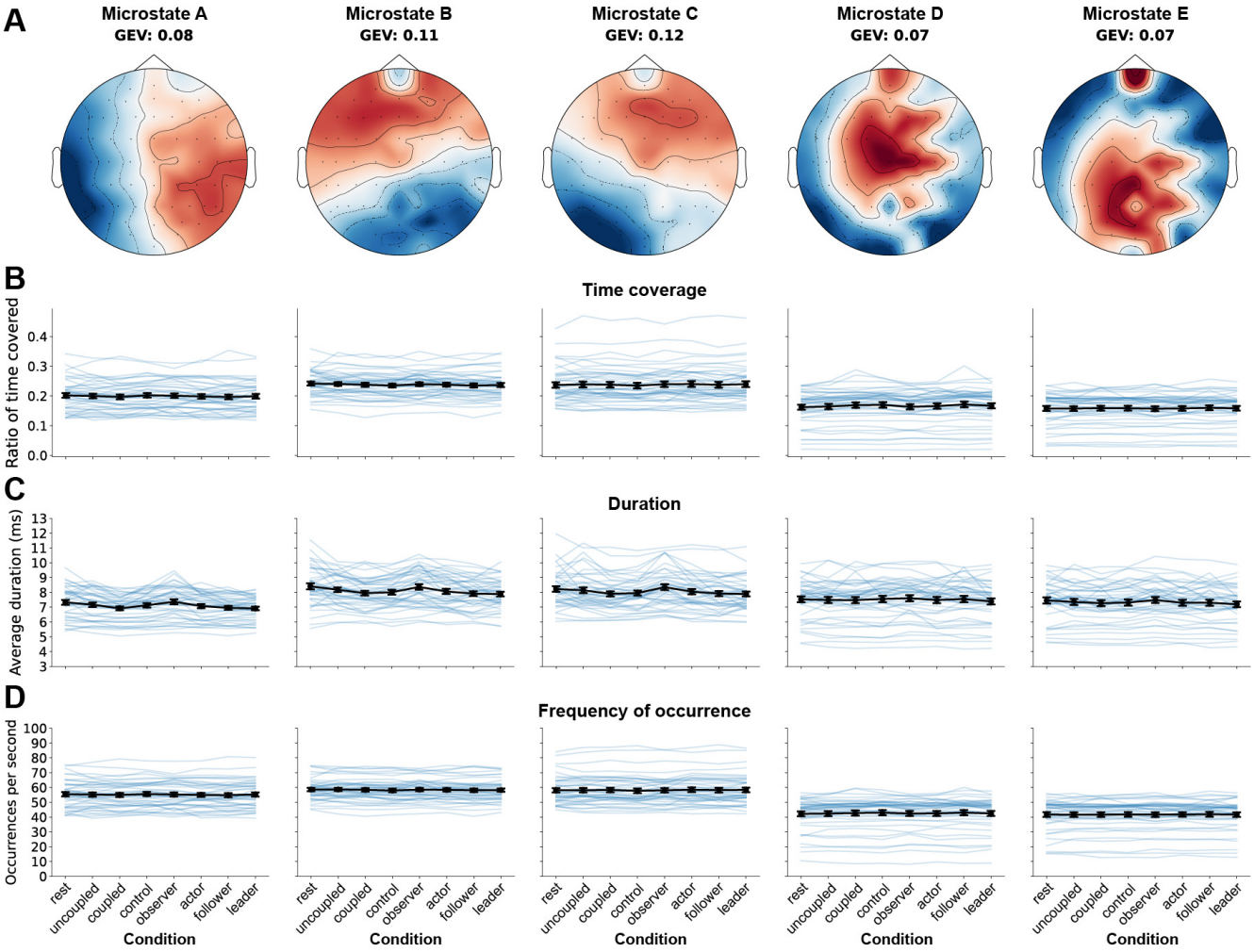

Fig. S2. **Conventional single-brain EEG broadband microstate analysis.** A) Microstate analysis was performed on the 42 individual EEG timeseries filtered in the broadband frequency range and five microstates were determined, which explained around 44% of the variance. B) The ratio of time covered of each microstate. C) The average duration of each microstate. D) The frequency of occurrence for each microstate. None of the features were related to the different behavioral conditions. GEV: global explained variance.

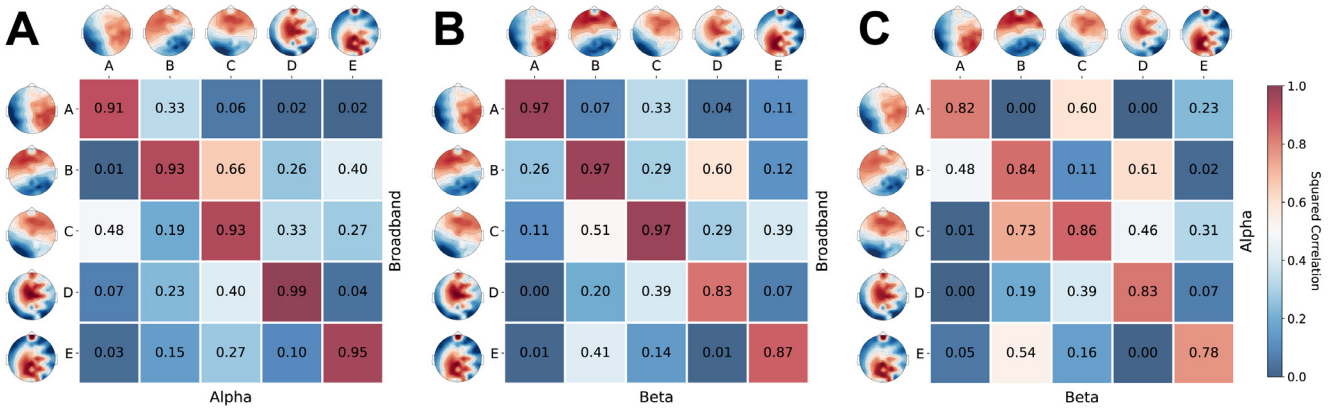

Fig. S3. **Spatial correlation between single-brain microstate topographies across frequencies.** The squared correlations between A) broadband and alpha, B) broadband and beta, and C) alpha and beta frequency ranges.

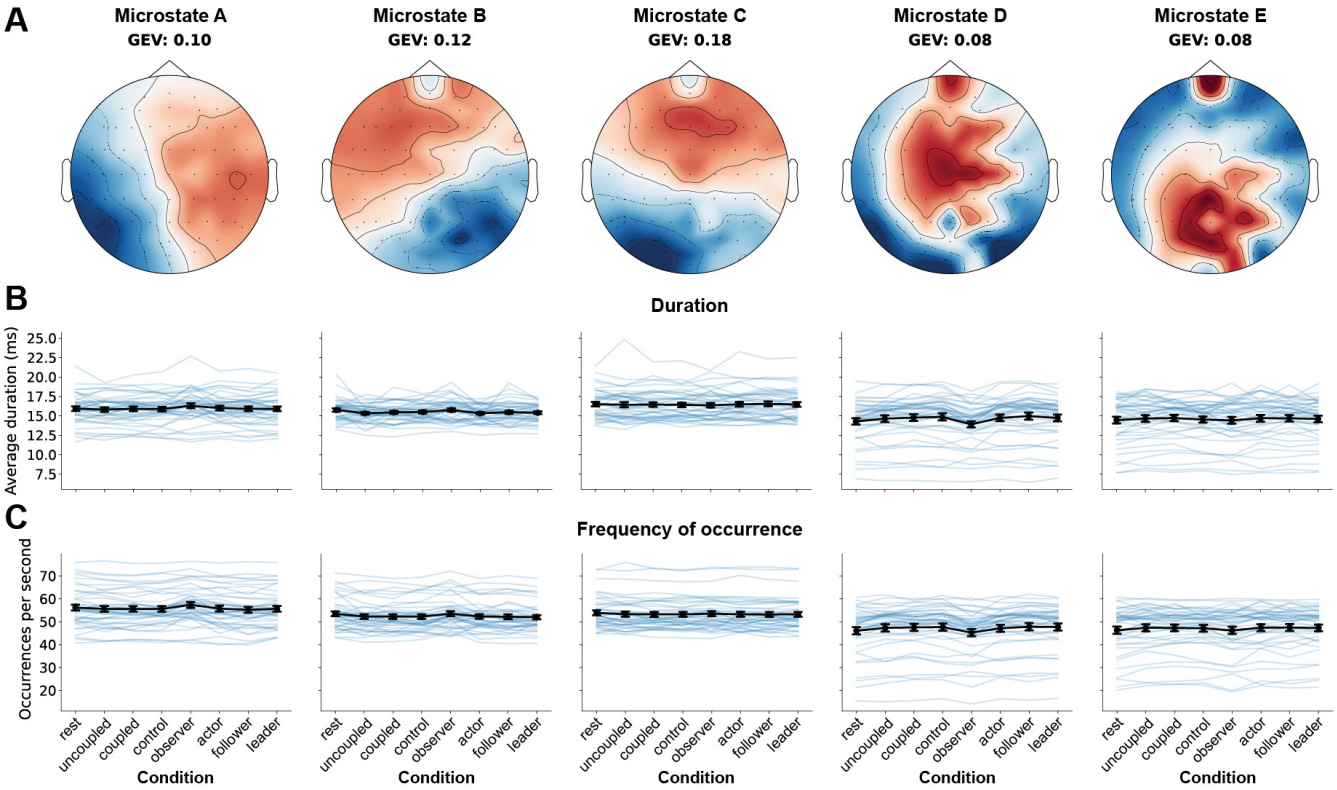

Fig. S4. **Conventional single-brain EEG alpha microstate analysis.** A) Microstate analysis was performed on the 42 individual EEG timeseries filtered in the alpha frequency range and five microstates were determined, which explained around 56% of the variance. B) The average duration of each microstate. C) The frequency of occurrence for each microstate. None of the features were related to the different behavioral conditions. GEV: global explained variance.

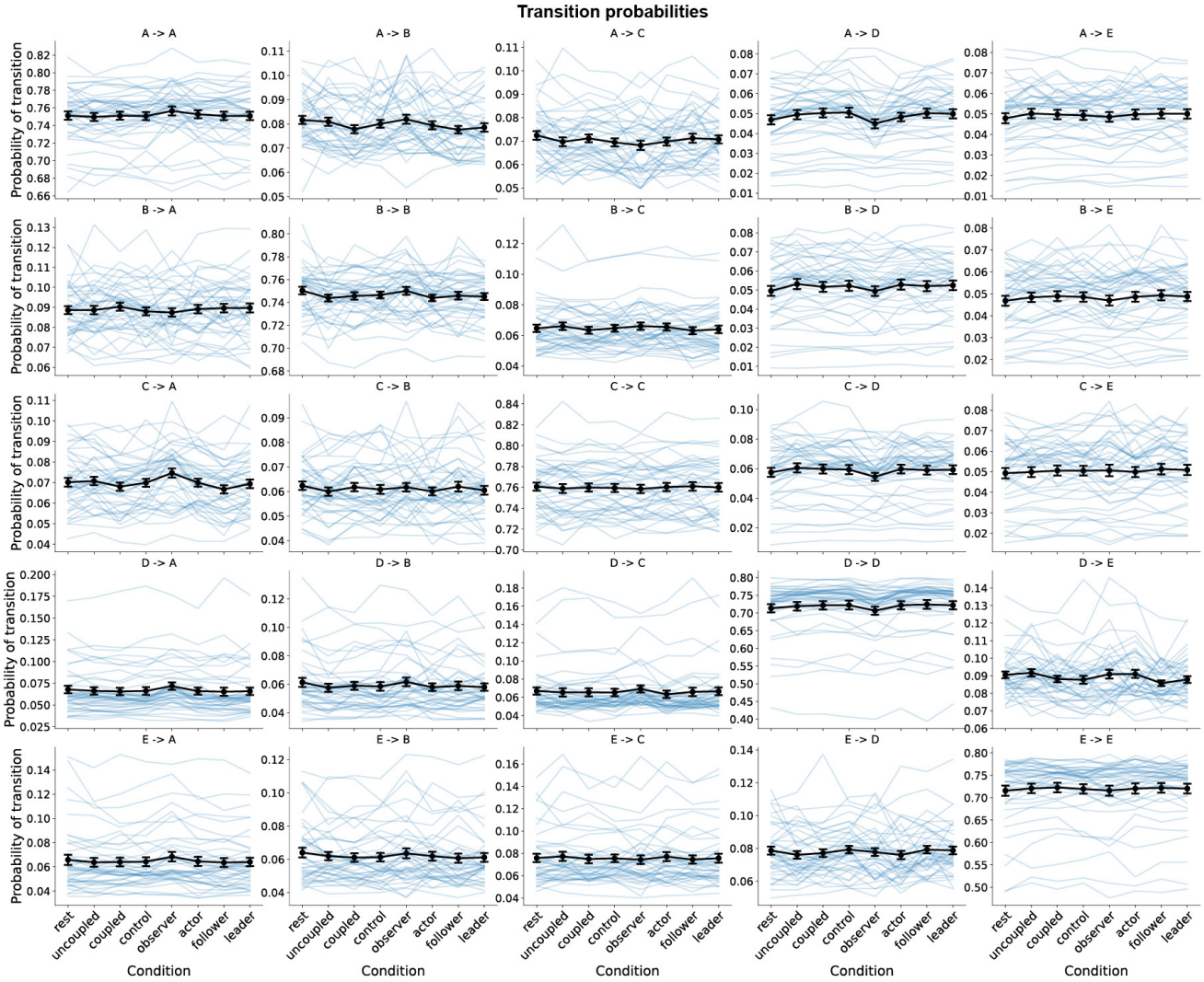

Fig. S5. **Single-brain alpha microstate transition probabilities.** The transition probabilities for single-brain alpha microstates. None of the features were related to the different behavioral conditions.

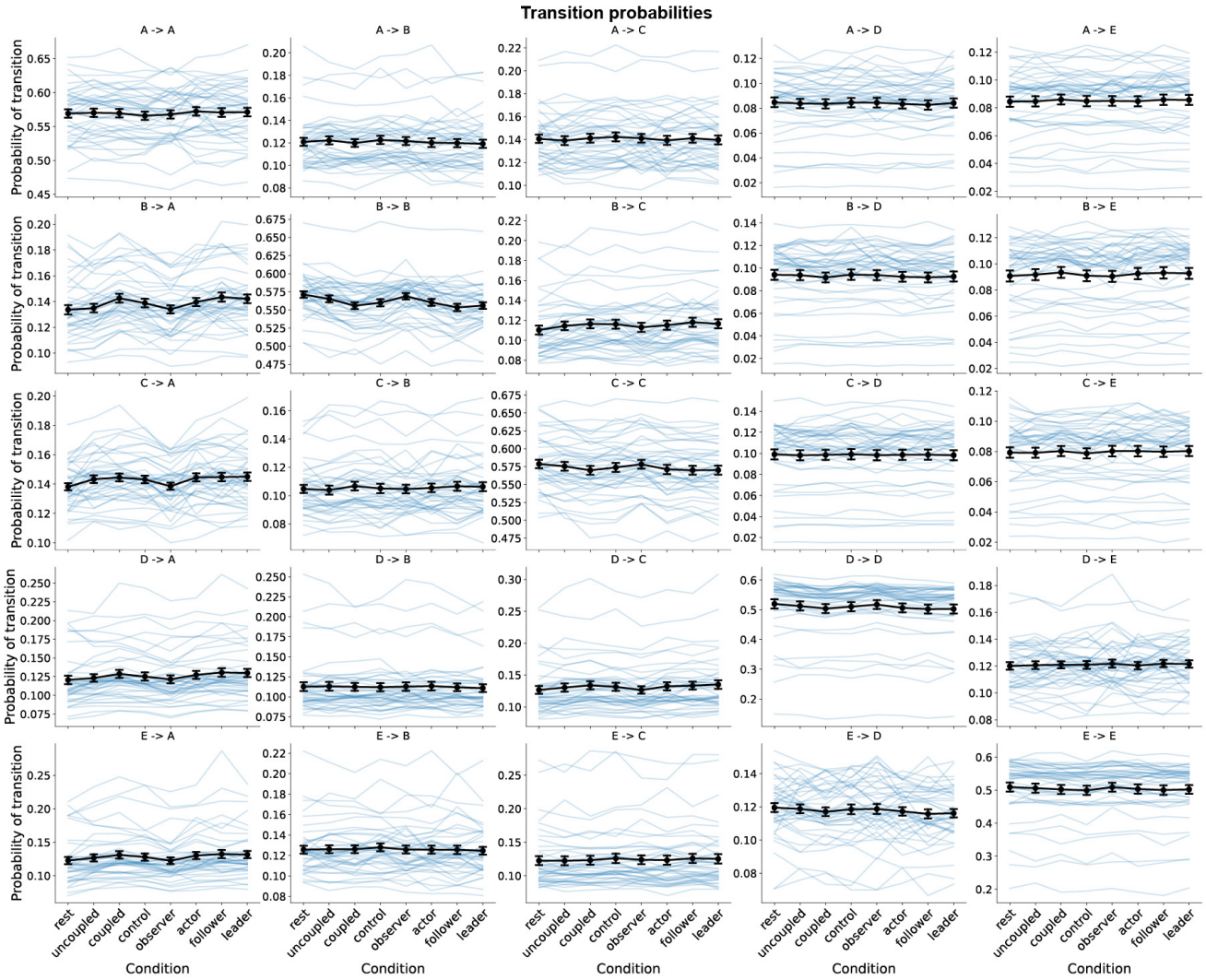

Fig. S6. **Single-brain beta microstate transition probabilities.** The transition probabilities for single-brain beta microstates. None of the features were related to the different behavioral conditions.

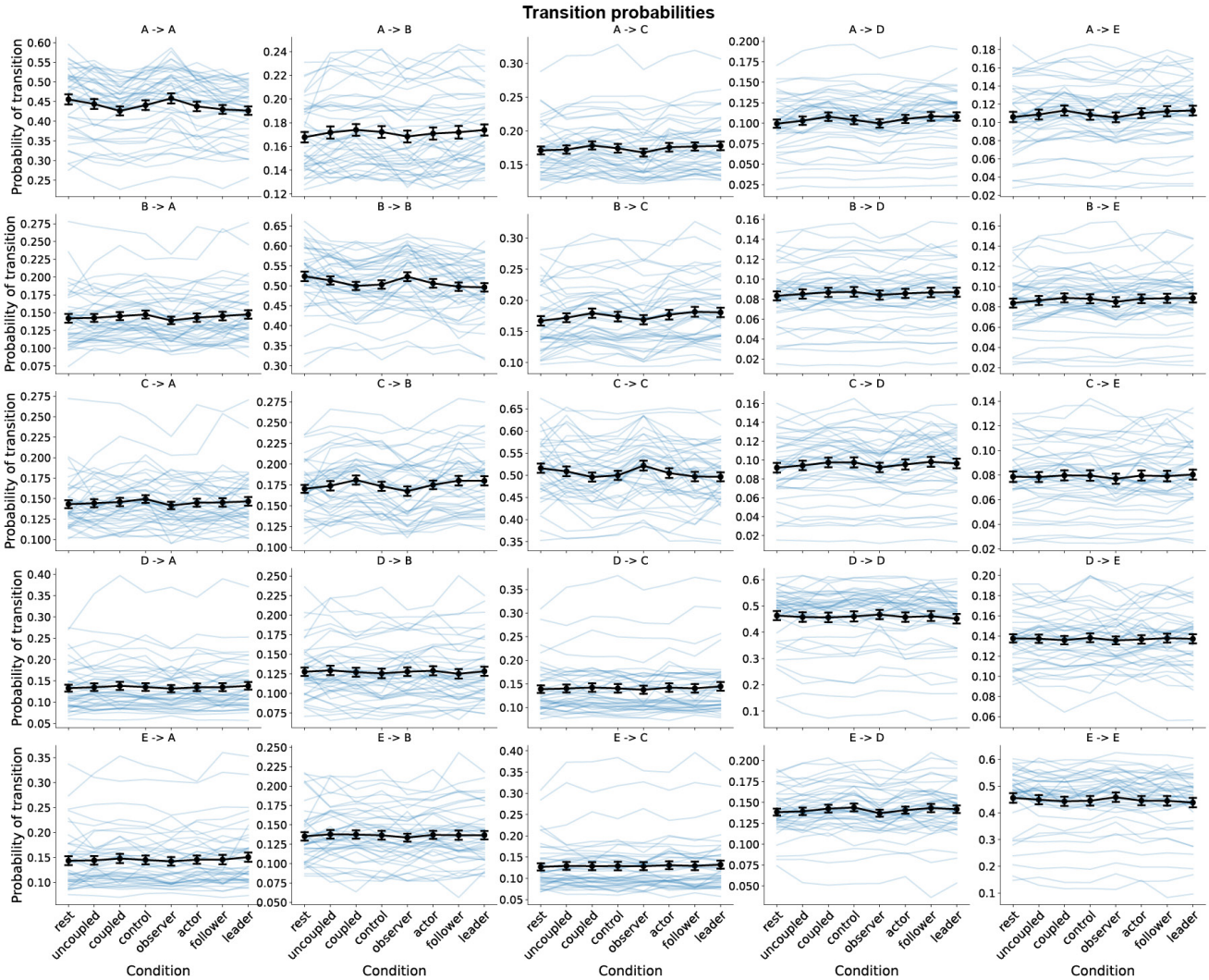

Fig. S7. **Single-brain broadband microstate transition probabilities.** The transition probabilities for single-brain broadband microstates. None of the features were related to the different behavioral conditions.

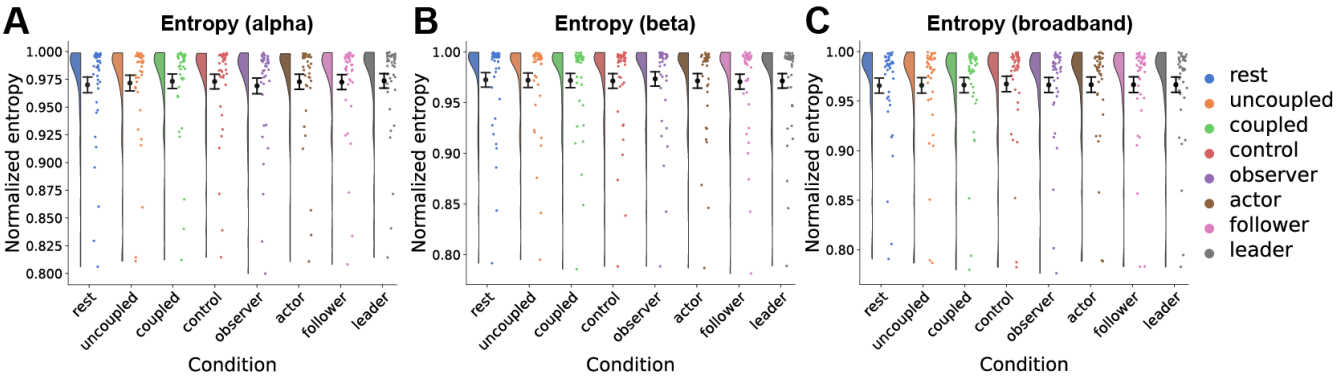

Fig. S8. **Single-brain EEG microstate entropy.** Shannon entropy was computed for the microstate sequence time series determined in the A) alpha, B) beta and C) broadband frequency range, normalized to the theoretical maximum (uniform label distribution). Entropy were not related to the different behavioral conditions.

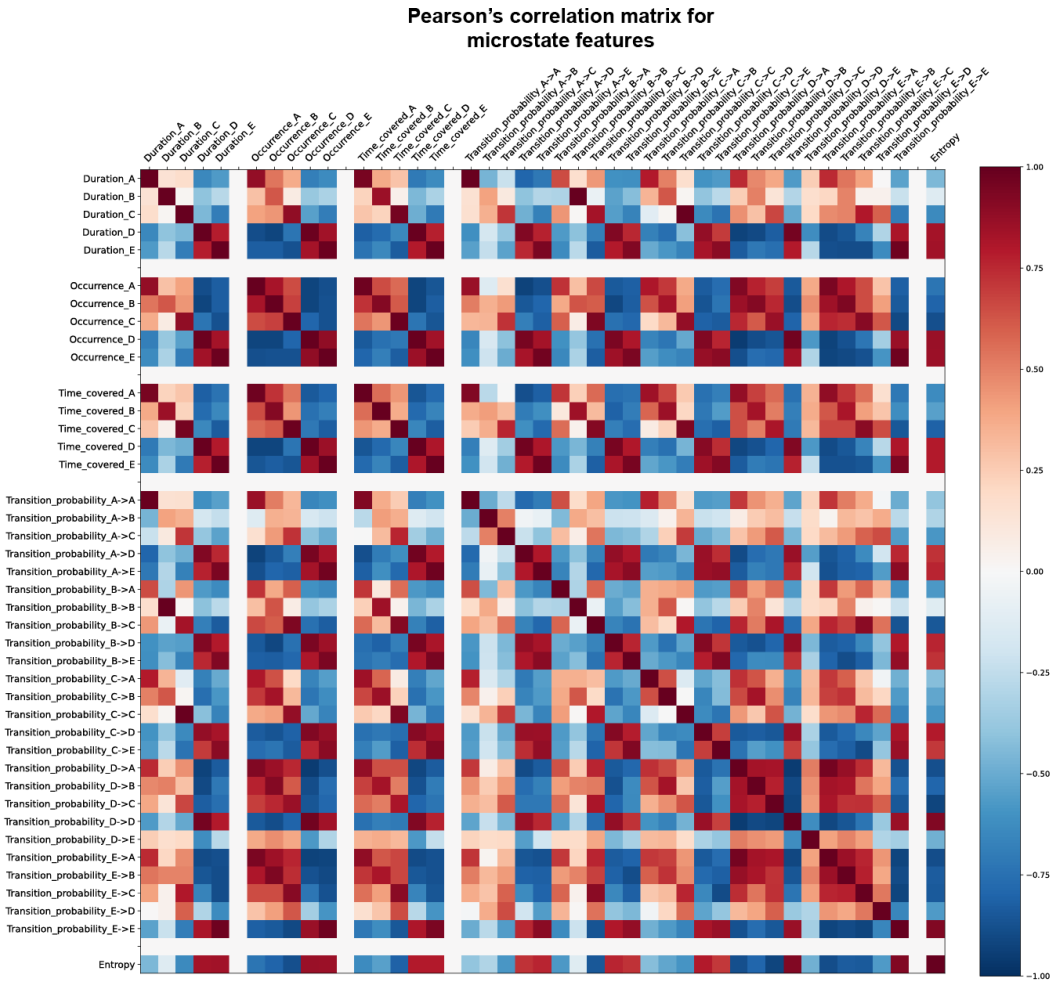

Fig. S9. **Pearson's correlation for single-brain EEG alpha microstate features.** Strong positive correlations are seen between microstate features corresponding to the same microstate. Microstate A, B and C are also often positively correlated, and the same is true for D, E, due to the high similarity in their corresponding topographic maps.

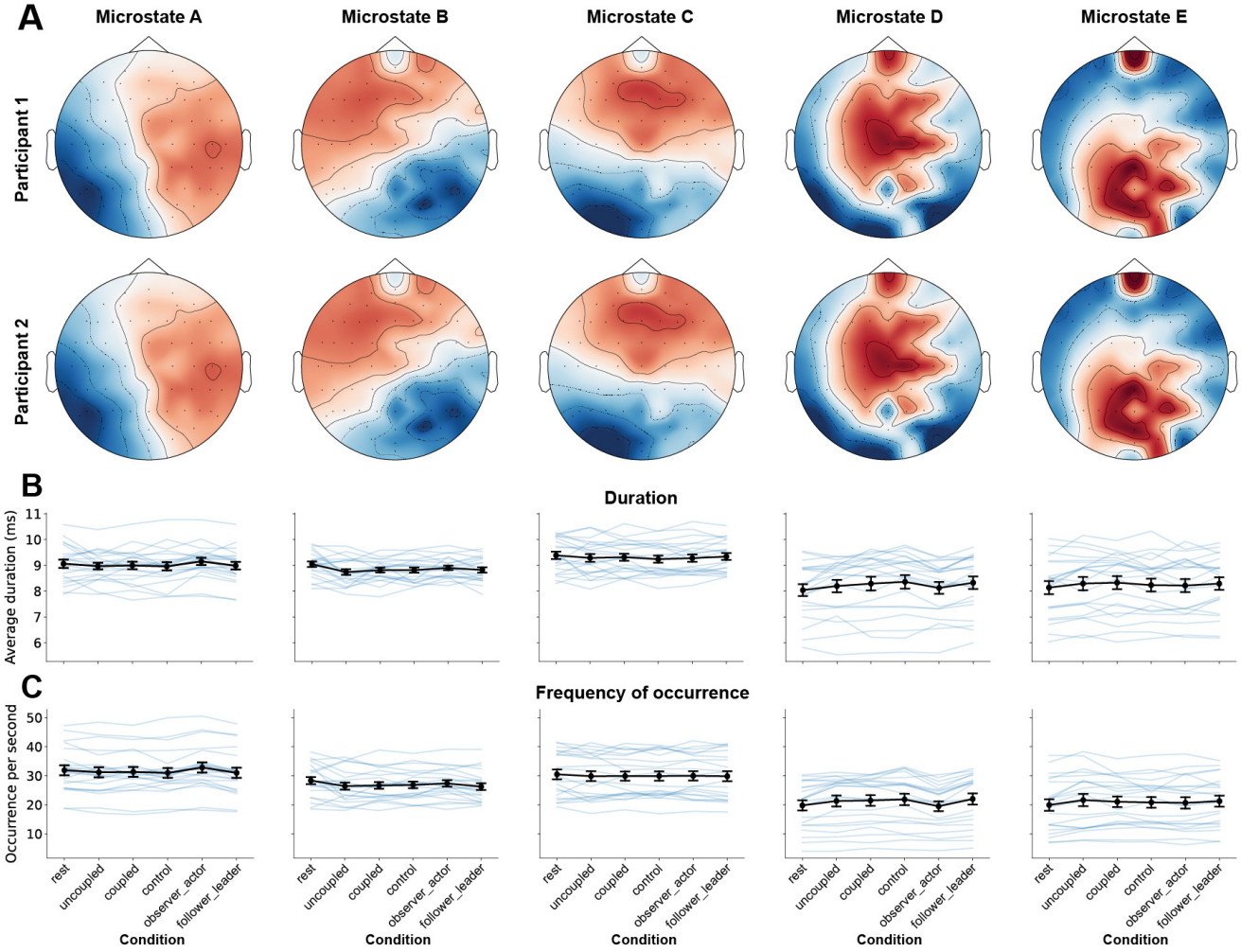

Fig. S10. **Inter-brain synchronization of alpha microstates.** A) We investigated the co-occurrence of similar alpha microstates in the two participants in the dyads. B) The average duration the participants were in the same microstate. C) The frequency of co-occurrence of each microstate. None of the features were related to the different behavioral conditions.

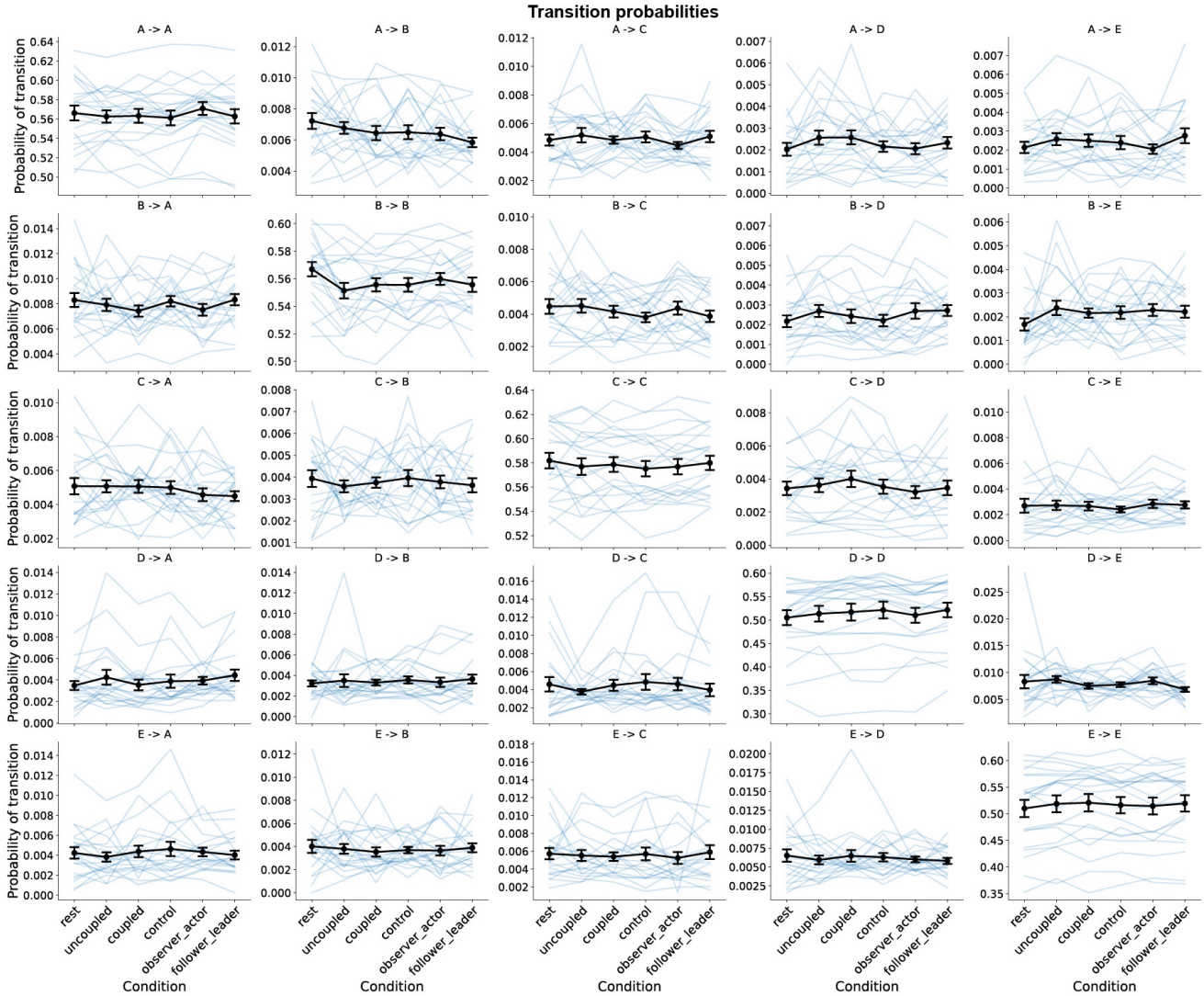

Fig. S11. **Inter-brain alpha microstate transition probabilities.** The transition probabilities for co-occurring inter-brain alpha microstates. None of the features were related to the different behavioral conditions.

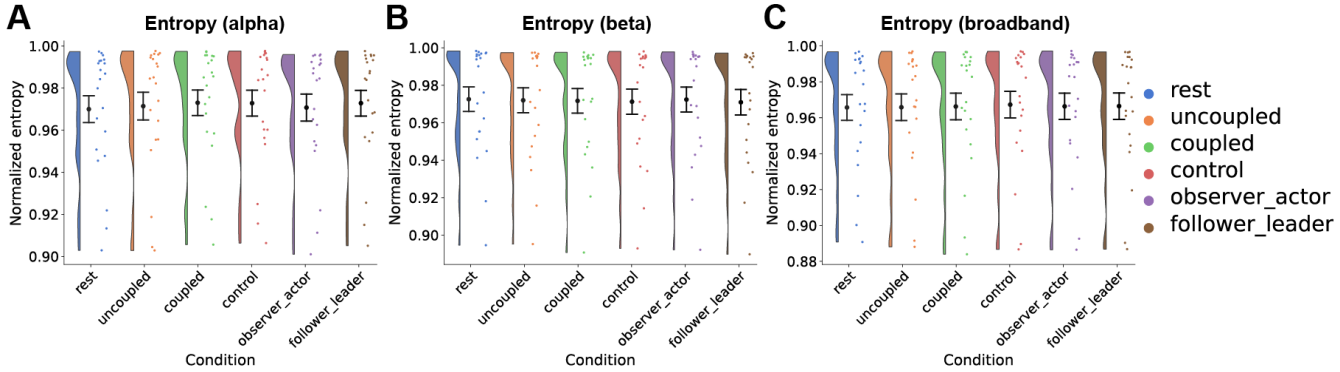

Fig. S12. **Inter-brain EEG microstate entropy.** Shannon entropy was computed for the sequence time series for co-occurring microstates determined in the A) alpha, B) beta and C) broadband frequency range, normalized to the theoretical maximum (uniform label distribution). Entropy were not related to the different behavioral conditions.

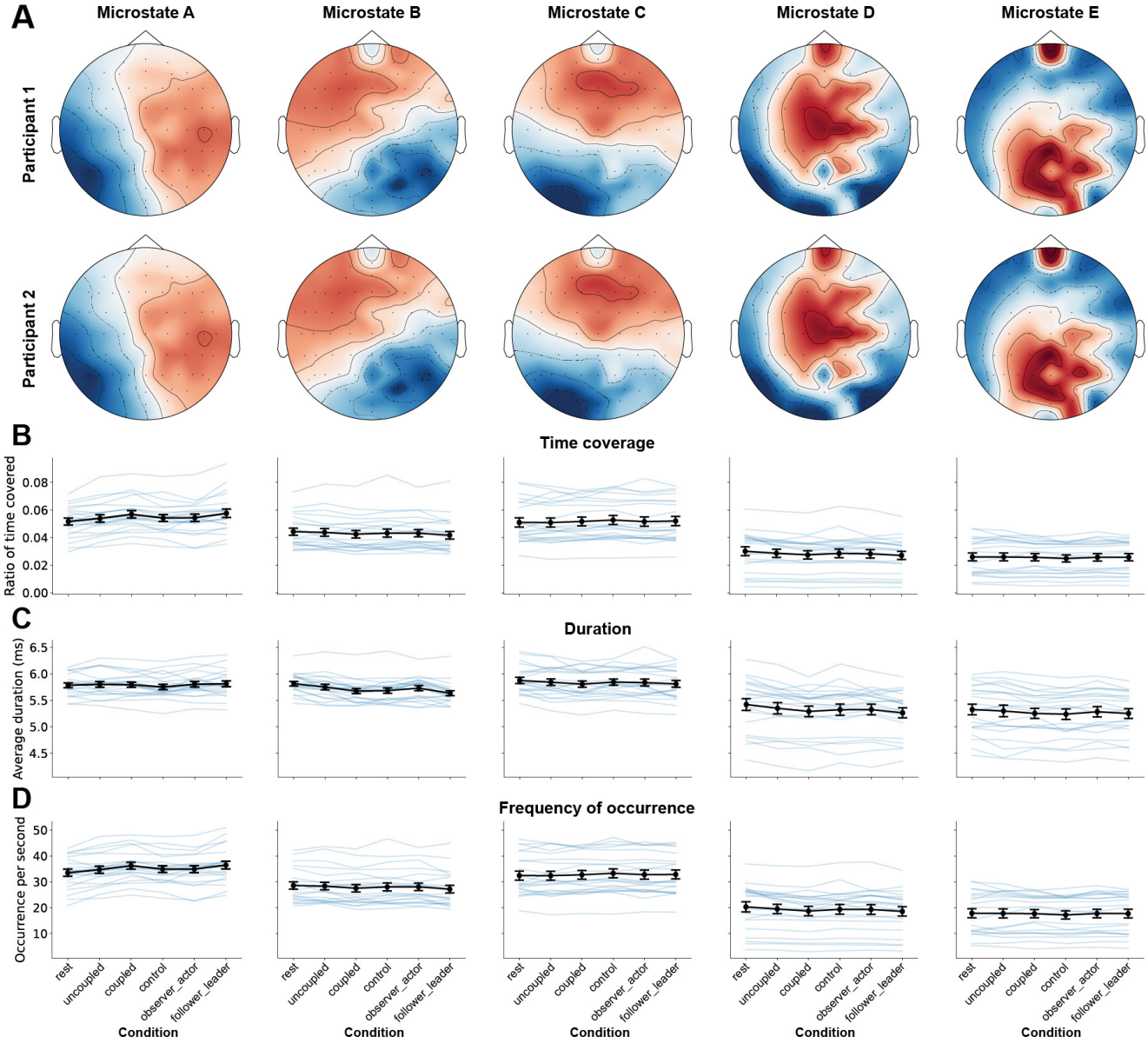

Fig. S13. **Inter-brain synchronization of beta microstates.** A) We investigated the co-occurrence of similar beta microstates in the two participants in the dyads. B) The ratio of time the participants were in the same microstate C) The average duration the participants were in the same microstate. D) The frequency of co-occurrence of each microstate. None of the features were related to the different behavioral conditions.

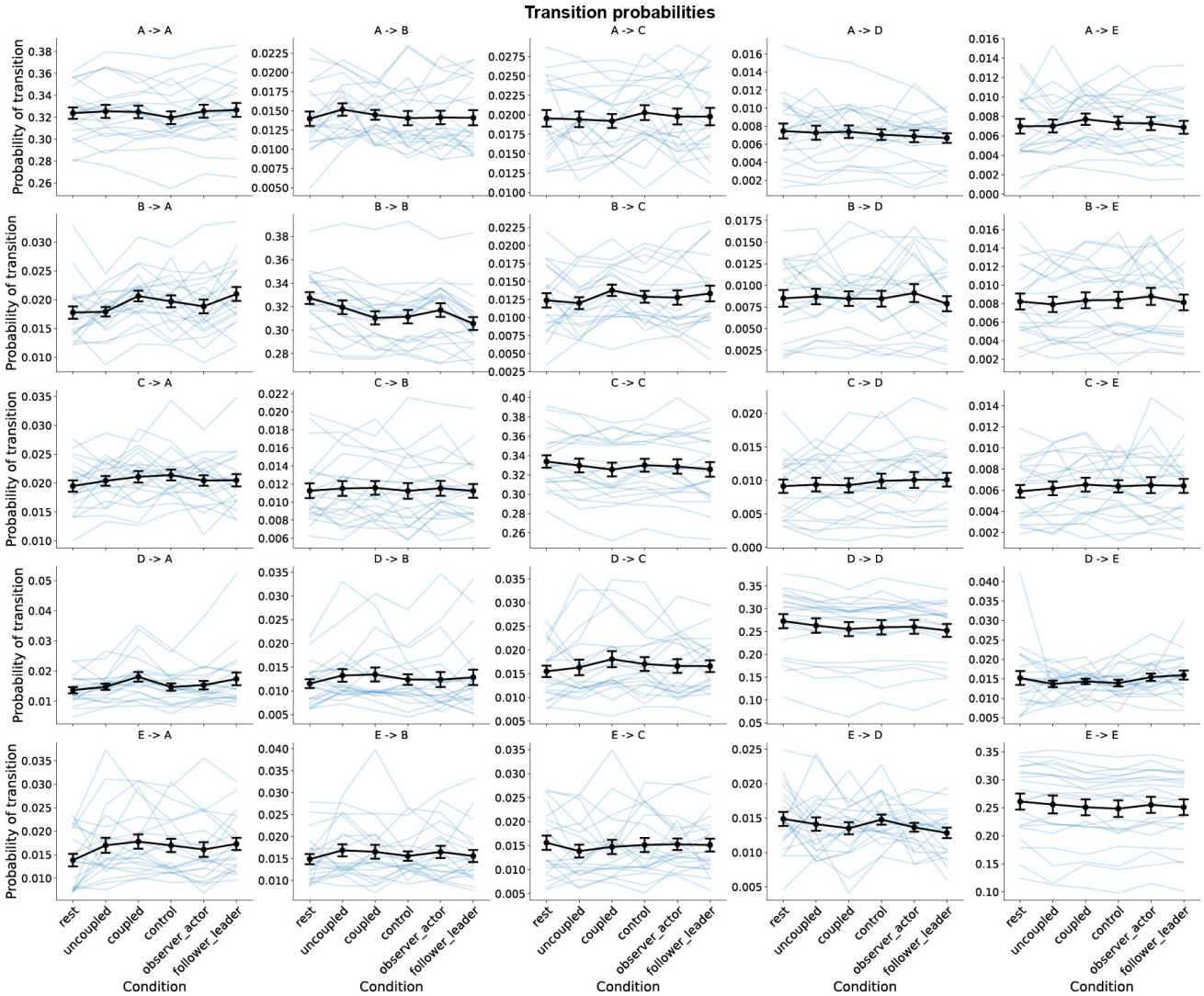

Fig. S14. **Inter-brain beta microstate transition probabilities.** The transition probabilities for co-occurring inter-brain beta microstates. None of the features were related to the different behavioral conditions.

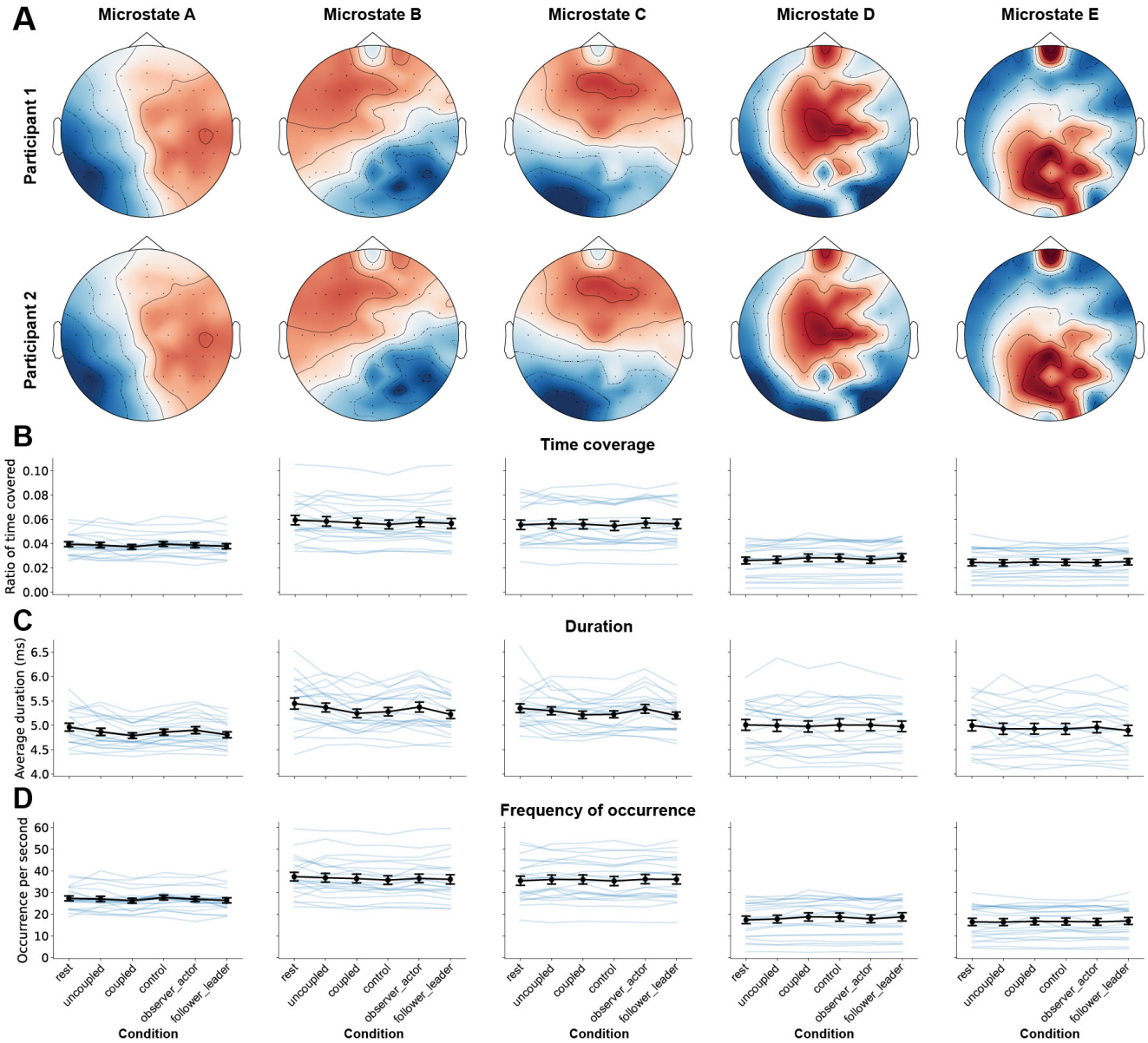

Fig. S15. **Inter-brain synchronization of broadband microstates.** A) We investigated the co-occurrence of similar broadband microstates in the two participants in the dyads. B) The ratio of time the participants were in the same microstate C) The average duration the participants were in the same microstate. D) The frequency of co-occurrence of each microstate. None of the features were related to the different behavioral conditions.

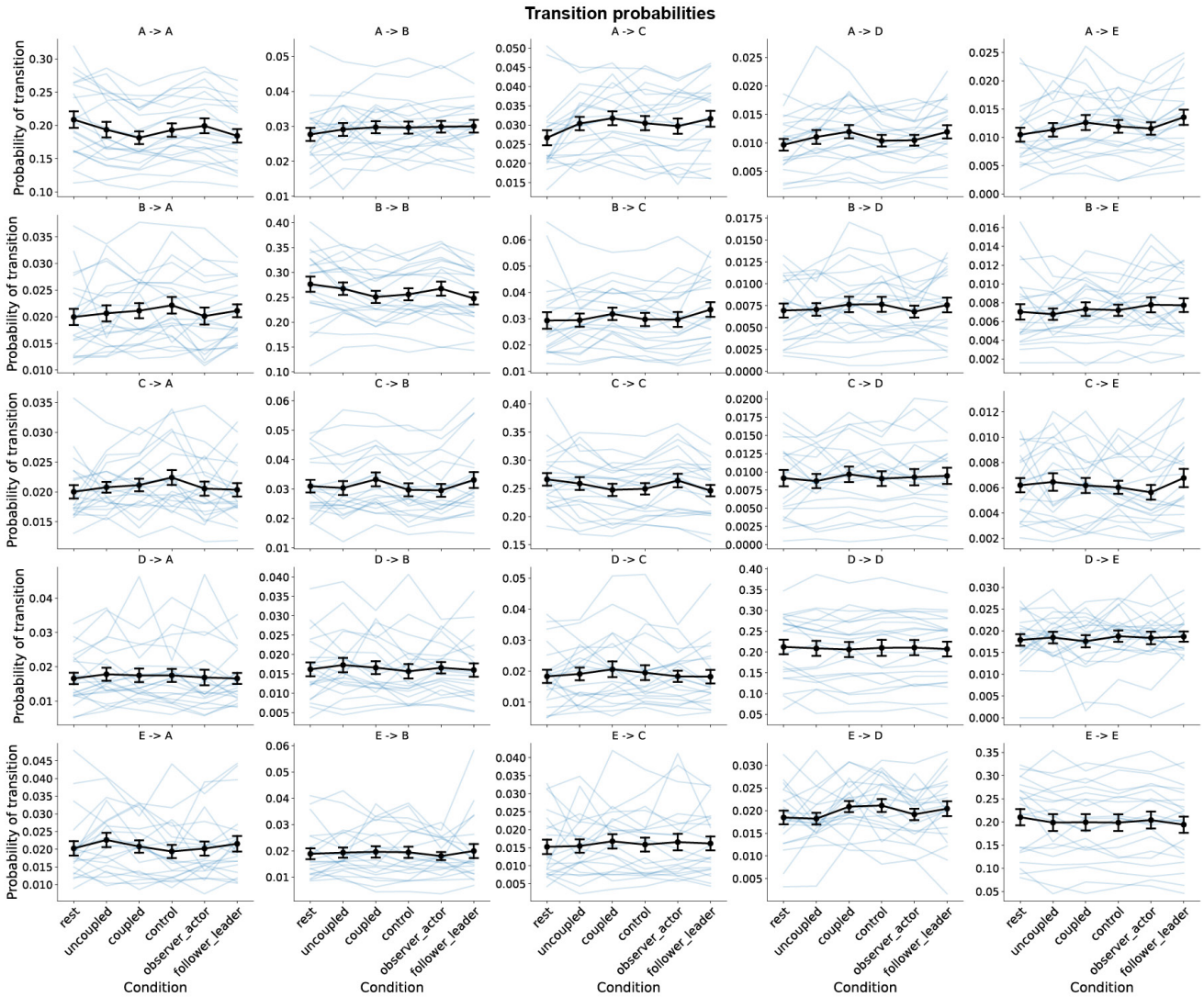

Fig. S16. **Inter-brain broadband microstate transition probabilities.** The transition probabilities for co-occurring inter-brain broadband microstates. None of the features were related to the different behavioral conditions.

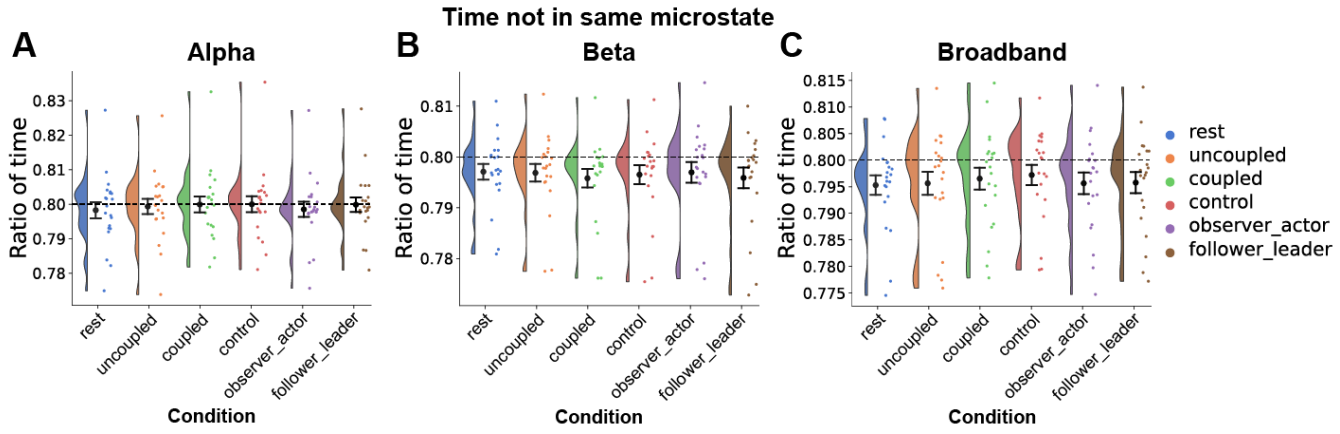

Fig. S17. **Ratio of time not in the same single-brain microstate.** We explored the option of estimating interbrain synchronization as the time dynamics of when the two individuals in a pair were in the same single-brain microstate. However, the pairs were rarely both in the same microstate, in fact the amount of time they were in the same microstate was around chance-level for both A) alpha microstates, B) beta microstates and C) broadband microstates. The dashed line indicates 0.80, which correspond to chance-level with 5 microstates.

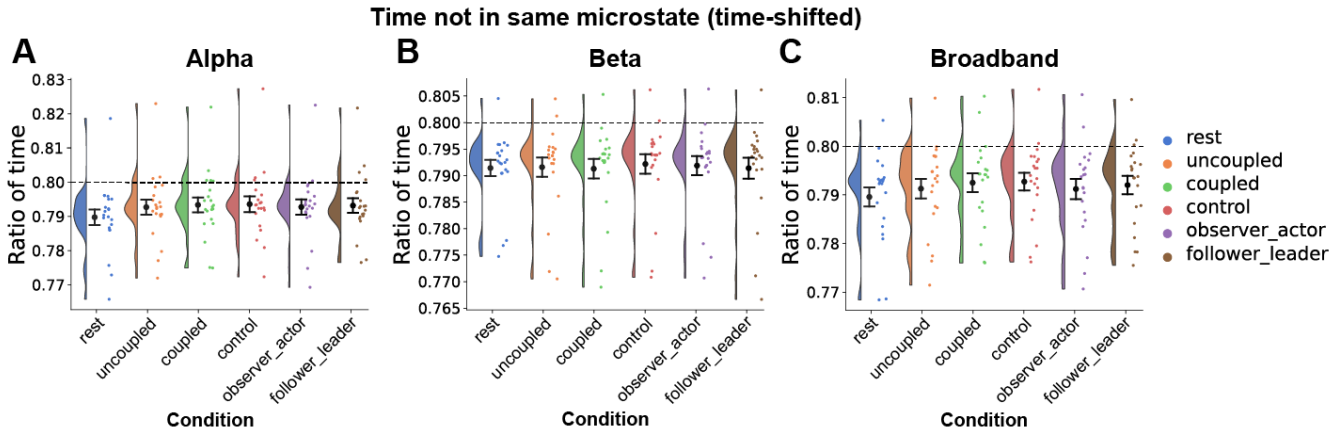

Fig. S18. **Ratio of time not in the same single-brain microstate, allowing for time-lags.** We explored whether similar microstates at not precisely time-locked, but lagged timepoints, resulted in increased inter-brain synchronization, however the decrease of ratio of time not in the same state was negligible for both A) alpha microstates, B) beta microstates and C) broadband microstates. The dashed line indicates 0.80, which correspond to chance-level with 5 microstates.

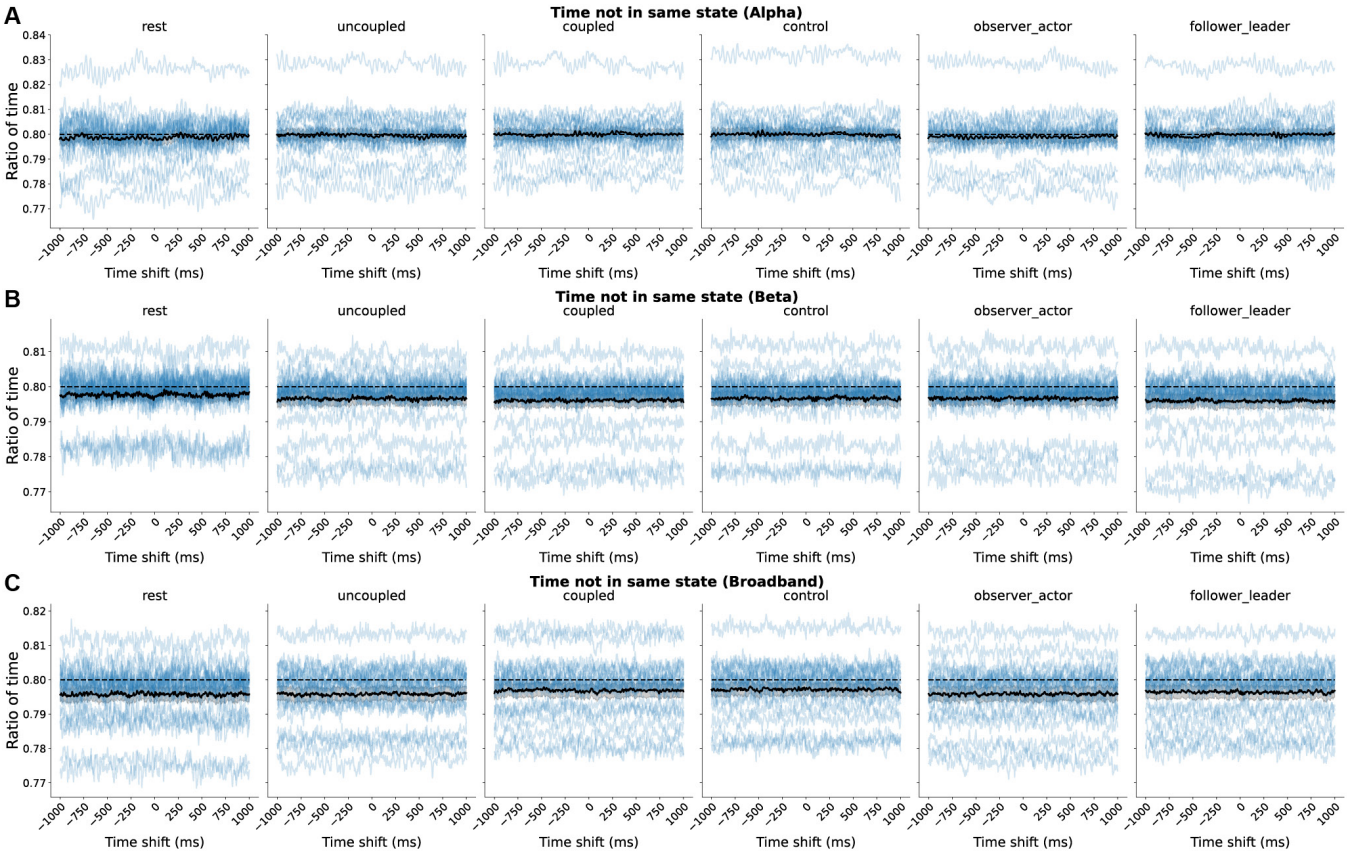

Fig. S19. **Ratio of time not in the same single-brain microstate at different time-lags.** No clear time-lag resulted in a increase in time-lagged inter-brain synchronization (decrease in ratio of time not in the same microstate) for both A) alpha microstates, B) beta microstates and C) broadband microstates. The dashed line indicates 0.80, which correspond to chance-level with 5 microstates. The black line indicates the mean, with each blue line corresponding to each dyad.

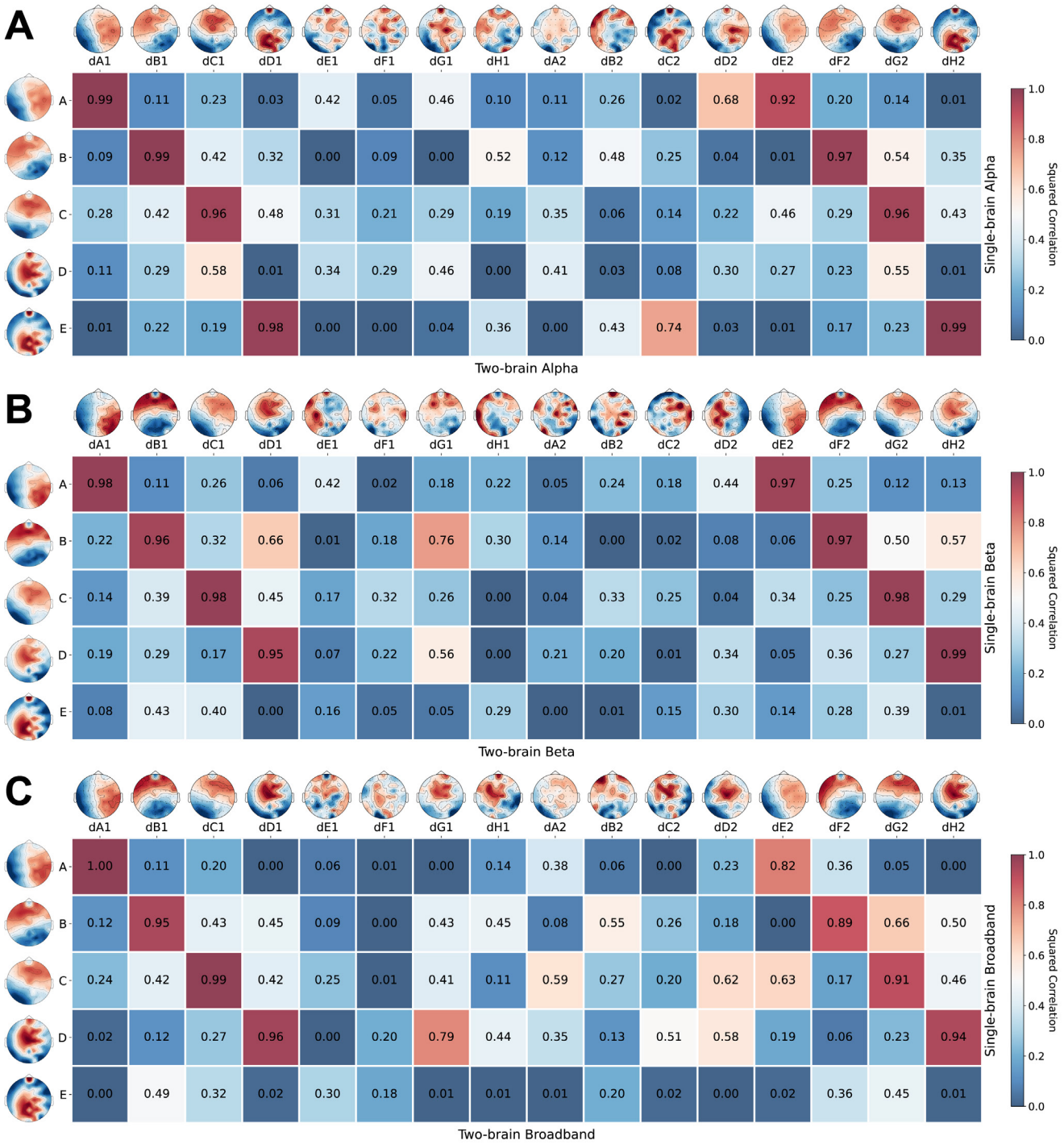

Fig. S20. **Spatial correlation between single-brain microstate and two-brain microstate topographies.** The squared correlations between the single-brain and two-brain microstates topographies in A) alpha, B) beta, and C) broadband frequency ranges.

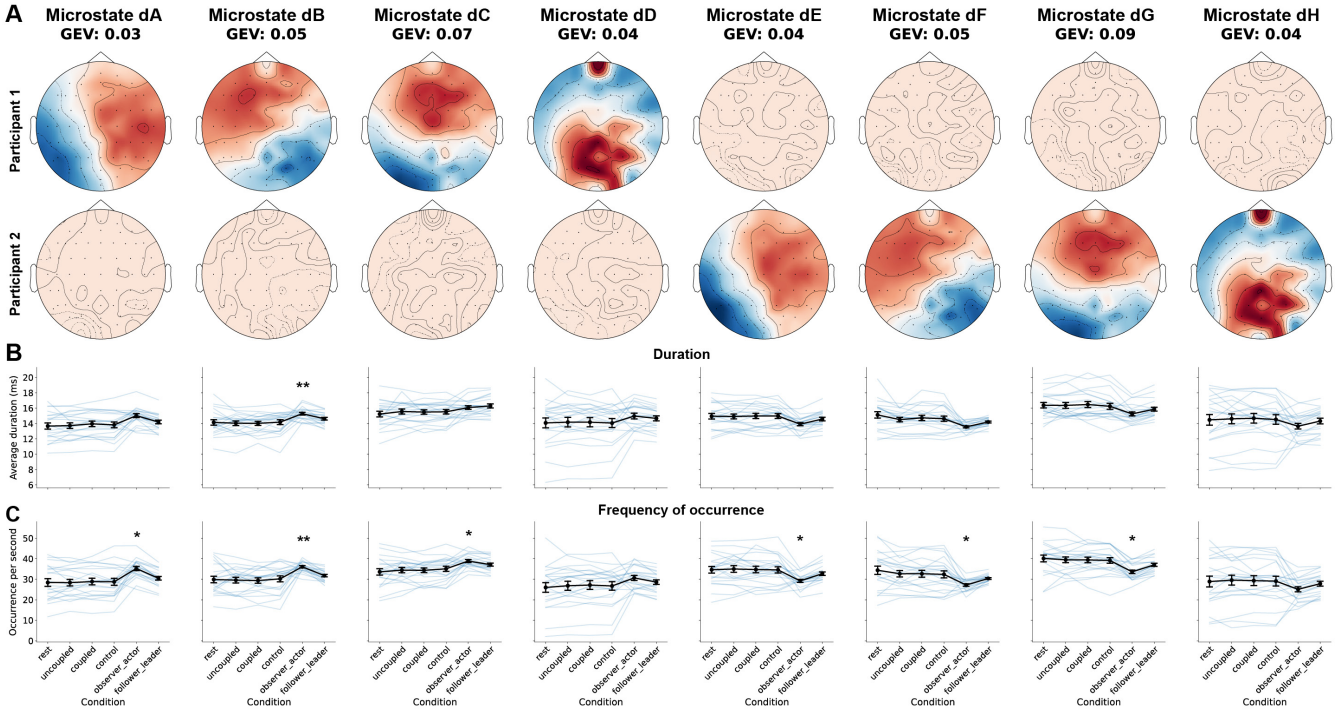

Fig. S21. **Two-brain alpha microstate analysis.** A) When the two-brain alpha microstates were plotted using a fixed color scale based on the the min and max value across all the microstates, it became evident that dA2, dB2, dC2, dD2, dE1, dF1, dG1 and dH1 reflected the mean topography, with a z-scored activity around 0. B) The average duration of each two-brain microstate. C) The frequency of occurrence for each two-brain microstate. Two-brain microstate dynamics were different between the asymmetrical observer-actor and symmetrical conditions. GEV: global explained variance.

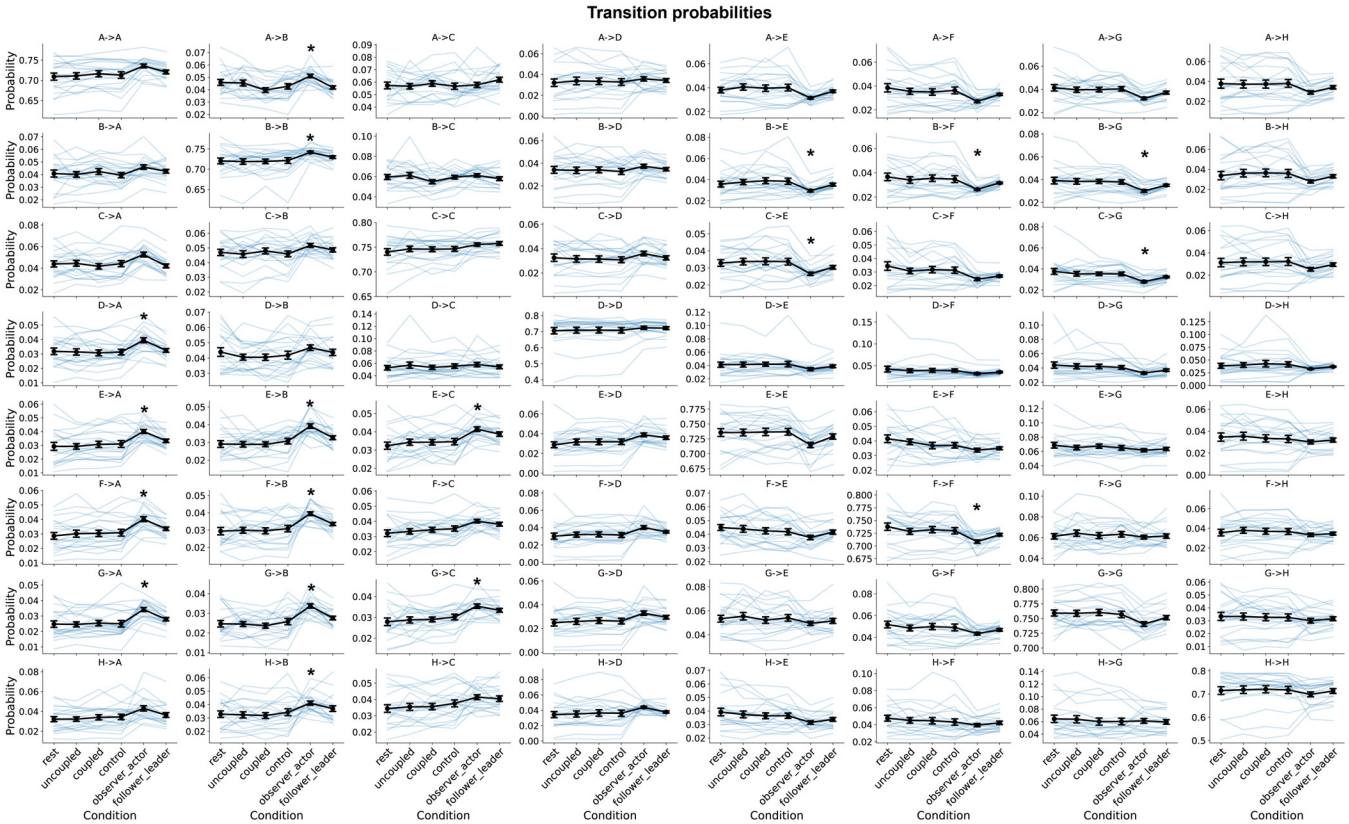

Fig. S22. **Two-brain alpha microstate transition probabilities.** Two-brain alpha microstate transition probabilities were different between the asymmetrical and symmetrical conditions, with only the observer-actor condition differing after multiple-comparison correction.

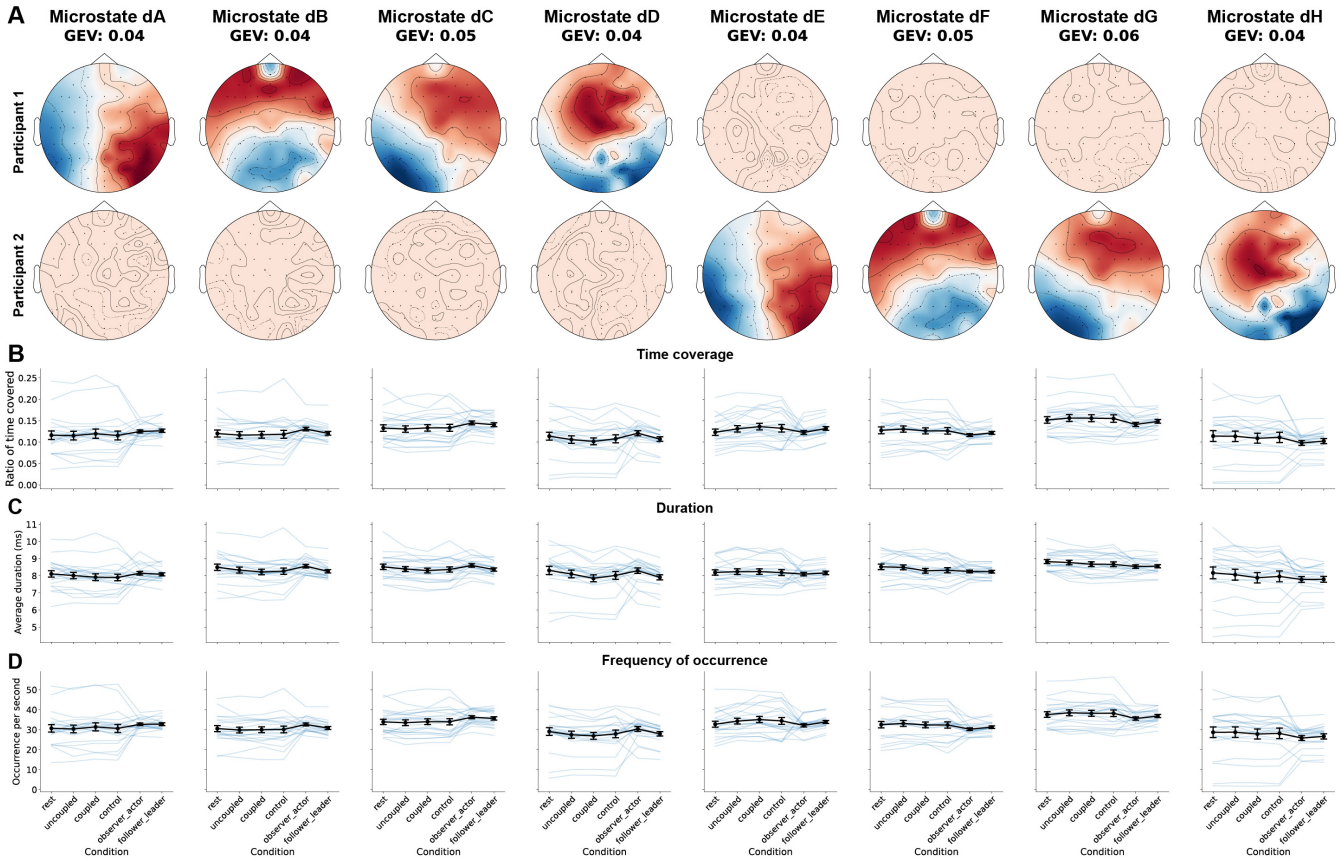

Fig. S23. **Two-brain beta microstate analysis.** A) Microstate analysis was performed on the simultaneously recorded EEG from 21 pairs collected during the mirror-game paradigm, which yielded eight two-brain beta microstates, explaining around 36% of the variance. B) The ratio of time covered by each two-brain microstate. C) The average duration of each two-brain microstate. D) The frequency of occurrence for each two-brain microstate. None of the features were related to the different behavioral conditions. GEV: global explained variance.

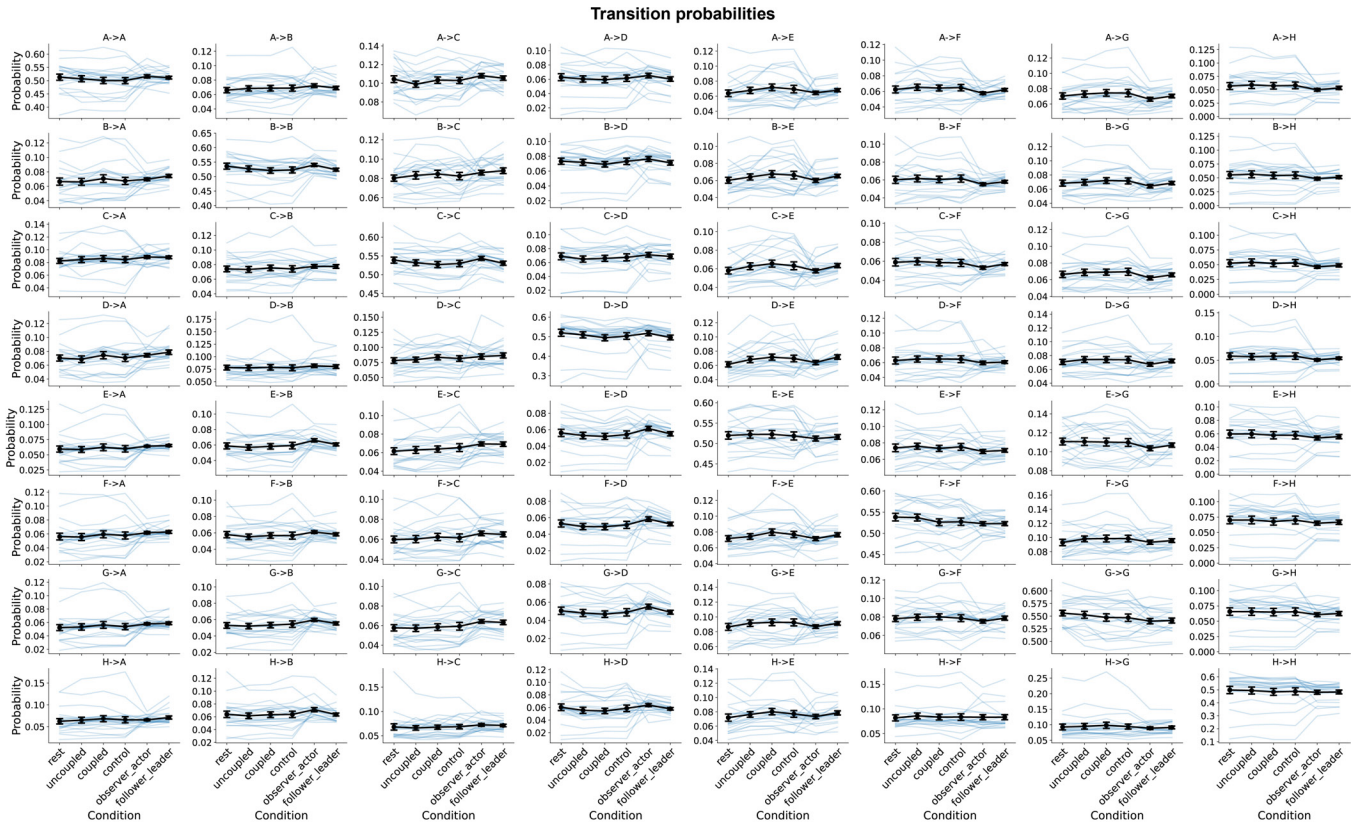

Fig. S24. **Two-brain beta microstate transition probabilities.** The probabilities of transitioning between each two-brain beta microstate were not related to the different behavioral conditions after multiple-comparison correction.

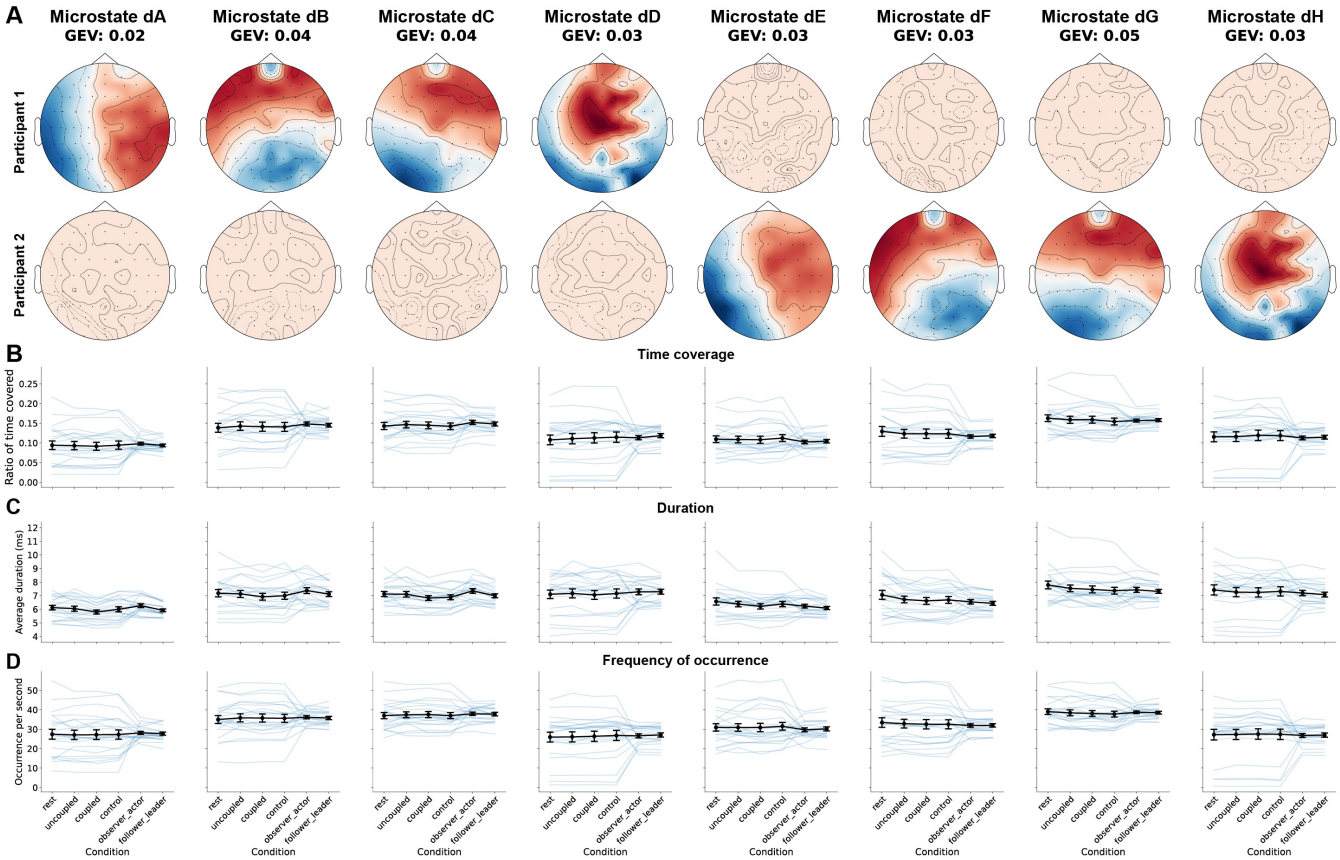

Fig. S25. **Two-brain broadband microstate analysis.** A) Microstate analysis was performed on the simultaneously recorded EEG from 21 pairs collected during the mirror-game paradigm, which yielded eight two-brain broadband microstates, explaining around 27% of the variance. B) The ratio of time covered by each two-brain microstate. C) The average duration of each two-brain microstate. D) The frequency of occurrence for each two-brain microstate. None of the features were related to the different behavioral conditions after multiple-comparison correction. GEV: global explained variance.

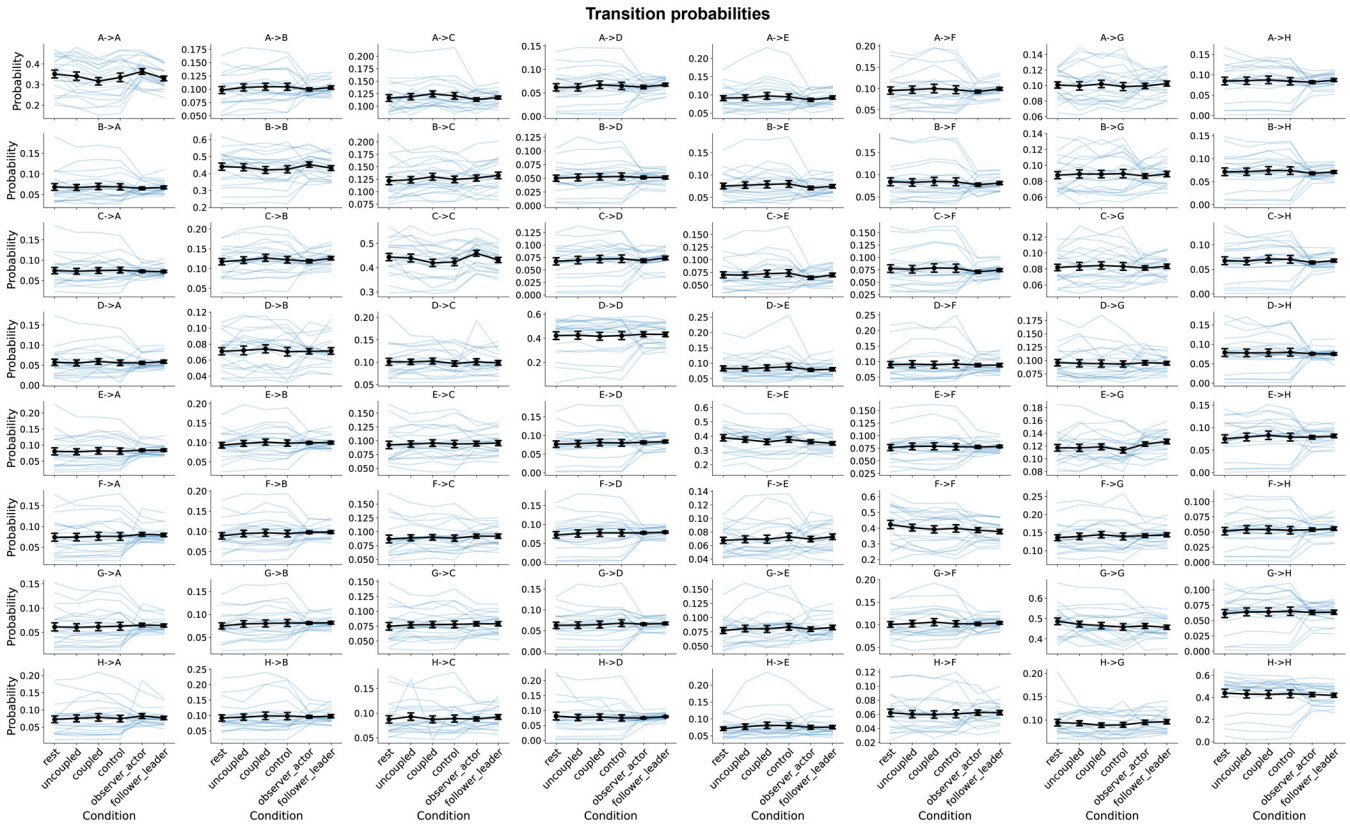

Fig. S26. **Two-brain broadband microstate transition probabilities.** The probabilities of transitioning between each two-brain broadband microstate were not related to the different behavioral conditions after multiple-comparison correction.

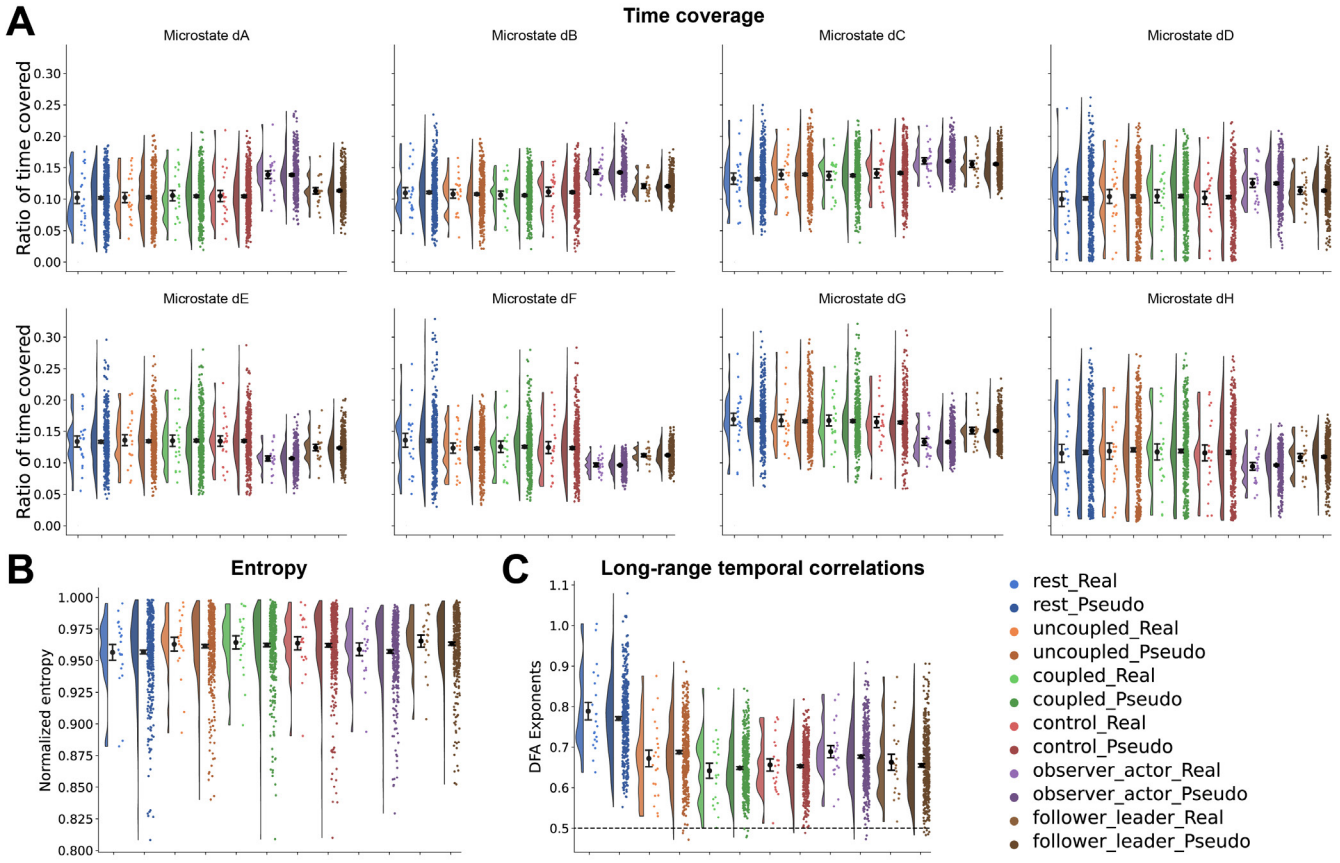

Fig. S27. **Two-brain microstate dynamics were similar between real pairs and pseudo-pairs.** The features shown are for the alpha frequency band. A) The time coverage was greater in dA, dB, dC and dD and lower in dE, dF, dG and dH in the asymmetrical tasks compared to principal symmetric *coupled* condition, however the difference was similar between the real pairs and the pseudo-pairs. The microstate sequence time series of the pseudo-pairs also had similar B) entropy and C) long-range temporal correlation as the real pairs. The colors correspond to each condition, with darker shades corresponding to the pseudo-pairs.

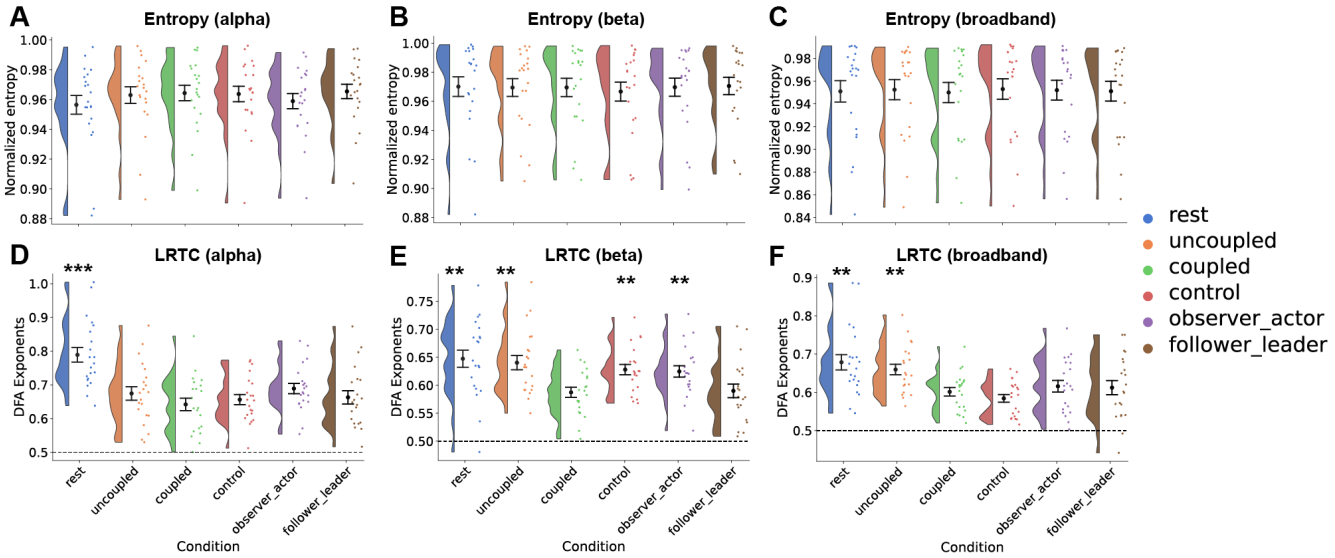

Fig. S28. **Complexity measures for two-brain EEG microstates.** Shannon entropy was computed for the microstate sequence time series, normalized to the theoretical maximum (uniform label distribution), for the A) alpha, B) beta and C) broadband frequency range. Long-range temporal correlations in the form of Hurst exponents were estimated as DFA exponents in the D) alpha, E) beta and F) broadband frequency range. Entropy features were not related to the different behavioral conditions, however the rest condition had significantly higher DFA exponents than the baseline coupled condition for all three frequency ranges, while uncoupled also had higher DFA exponents than coupled in the beta and broadband frequency range. The control and observer-actor condition was also associated with higher DFA exponents than the coupled condition in the beta frequency range. GEV: global explained variance, DFA: detrended fluctuation analysis. To perform DFA on the microstate label time series, dA, dB, dC and dD was partitioned into class 1 and dE, dF, dG and dH into class 2. DFA: detrended fluctuation analysis, LRTC: long-range temporal correlations.

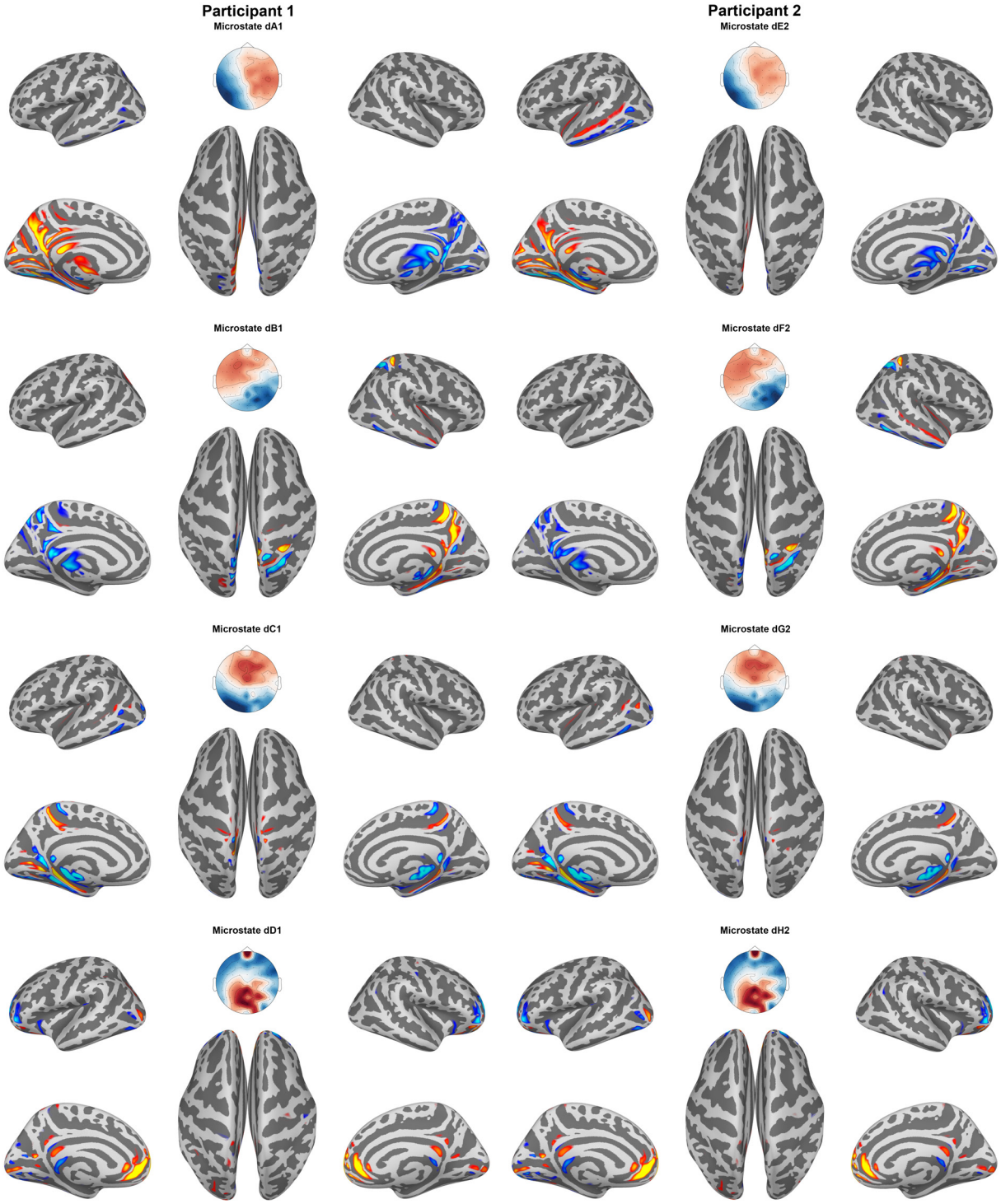

Fig. S29. **The eight two-brain microstates and their corresponding eLORETA cortical activities.** We only showed the cortical sources for dA1, dB1, dC1, dD1, dE2, dF2, dG2 and dH2 as the other two-brain microstates reflected the mean arbitrary activity (i.e. had no noticeable areas of activity).

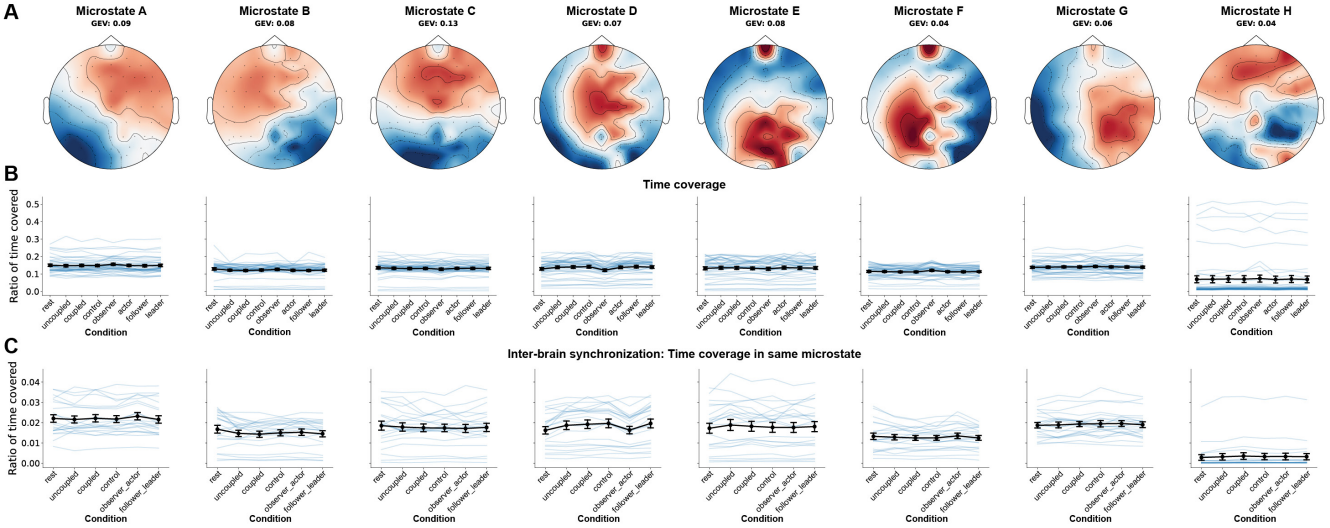

Fig. S30. **Single-brain EEG microstate analysis with eight extracted microstates.** A) To be consistent with the eight extracted microstates for the two-brain microstate analysis, we repeated the single-brain microstate analysis using the same cluster number. In total, the eight microstates explained around 60% of the variance. B) The ratio of time covered by each microstate was not related to the different behavioral conditions. C) The ratio of time the two participants in a dyad were in the same microstate was also not related to the different behavioral conditions. Notice the ratio of time coverage in C) was normalized to the total time they were in the same microstate and the time not in the same microstate (Supplementary Figure S17). GEV, global explained variance.

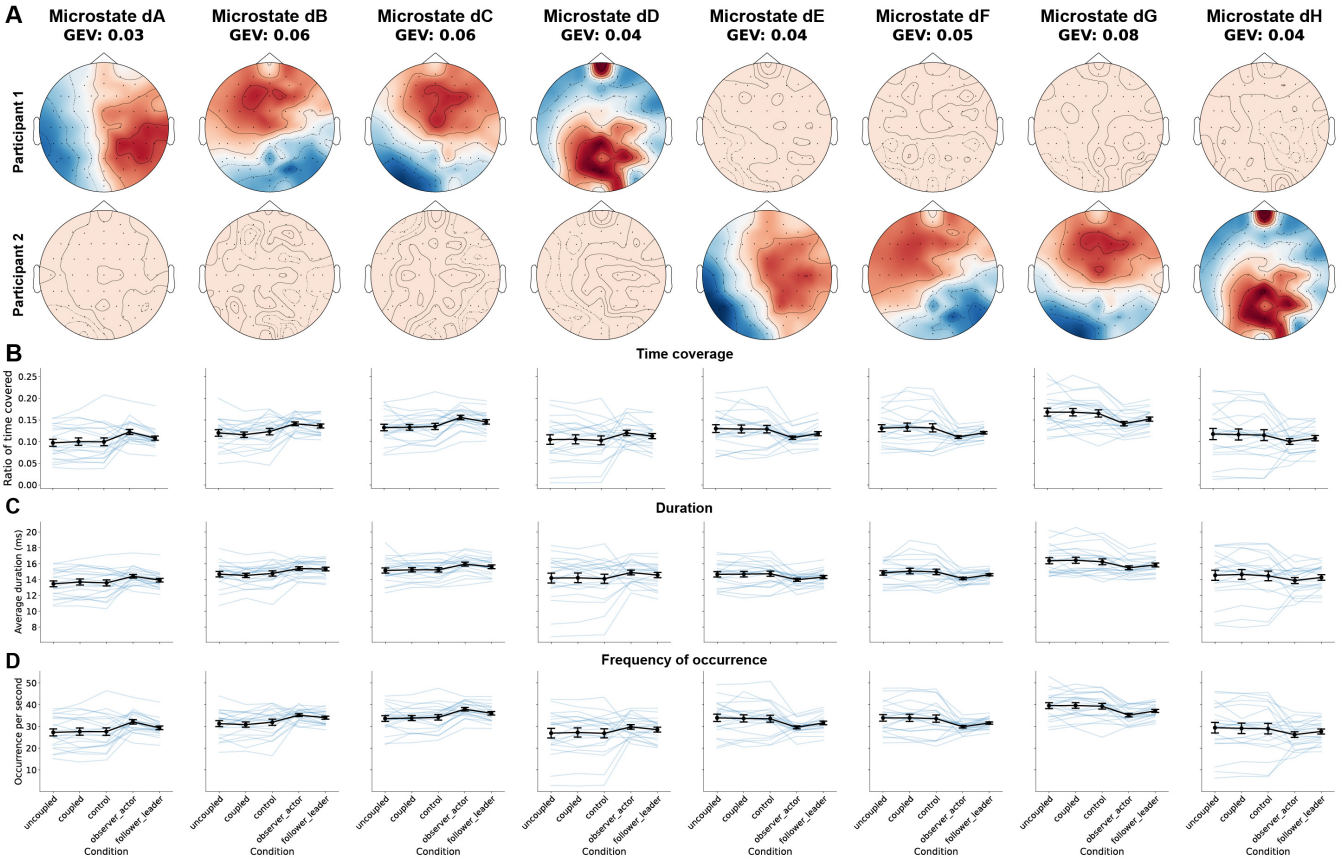

Fig. S31. **Removing rest conditions did not change the determined two-brain microstates.** A) We repeated the two-brain alpha microstate fitting after excluding the rest conditions. No clear qualitative differences were observed. B) The ratio of time covered by each two-brain microstate fitted without rest conditions showed the same trends with greater time coverage of canonical resting-state-like microstates in the observer (dA, dB, dC and dD) and lower time coverage in the observer (dE, dF, dG and dH). GEV: global explained variance.